HHS Public Access

Author manuscript

Toxicol Appl Pharmacol. Author manuscript; available in PMC 2016 September 01.

Published in final edited form as:

Toxicol Appl Pharmacol. 2015 September 1; 287(2): 149–160. doi:10.1016/j.taap.2015.05.019.

Cytochrome P450 1b1 in Polycyclic Aromatic Hydrocarbon (PAH)-Induced Skin Carcinogenesis: Tumorigenicity of Individual PAHs and Coal-Tar Extract, DNA Adduction and Expression of Select Genes in the *Cyp1b1* Knockout Mouse

Lisbeth K. Siddens[1,2], **Kristi L. Bunde**[5], **Tod A. Harper Jr**[1,3,4], **Tammie J. McQuistan**[2,3], **Christiane V. Löhr**[4,5], **Lisa M. Bramer**[6], **M. Waters Katrina**[2,7], **Susan C. Tilton**[1,2], **Sharon K. Krueger**[1,2,3], **David E. Williams**[*,1,2,3,4], and **William M. Baird**[1,2,4]

[1]Department of Environmental and Molecular Toxicology, Oregon State University, Corvallis, OR 97331, USA

[2]Superfund Research Center, Oregon State University, Corvallis, OR 97331, USA

[3]Linus Pauling Institute, Oregon State University, Corvallis, OR 97331, USA

[4]Environmental Health Sciences Center, Oregon State University, Corvallis, OR 97331, USA

[5]College of Veterinary Medicine, Oregon State University, Corvallis, OR 97331, USA

[6]Applied Statistics and Computational Modeling, Pacific Northwest National Laboratory, Richland, WA 99352, USA

[7]Biological Sciences Division, Pacific Northwest National Laboratory, Richland, WA 99352, USA

Abstract

FVB/N mice wild-type, heterozygous or null for *Cyp 1b1* were used in a two-stage skin tumor study comparing PAH, benzo[*a*]pyrene (BaP), dibenzo[*def*,*p*]chrysene (DBC), and coal tar extract (CTE, SRM 1597a). Following 20 weeks of promotion with TPA the *Cyp 1b1* null mice, initiated with DBC, exhibited reductions in incidence, multiplicity, and progression. None of these effects were observed with BaP or CTE. The mechanism of Cyp 1b1-dependent alteration of DBC skin carcinogenesis was further investigated by determining expression of select genes in skin from DBC-treated mice 2, 4 and 8 h post-initiation. A significant reduction in levels of *Cyp 1a1, Nqo1 at 8 h* and *Akr 1c14* mRNA was observed in *Cyp 1b1* null (but not wt or het) mice, whereas no impact was observed in *Gst a1, Nqo 1 at 2 and 4 h or Akr 1c19 at any time point*. *Cyp 1b1* mRNA was not elevated by DBC. The major covalent DNA adducts, dibenzo[*def*,*p*]chrysene-(±)-11,12-dihydrodiol-*cis* and *trans*-13,14-epoxide-deoxyadenosine (DBCDE-dA) were quantified by UHPLC-MS/MS 8 h post-initiation. Loss of *Cyp1 b1* expression reduced DBCDE-dA adducts in skin but not to a statistically significant degree. The ratio of *cis*-to *trans*-DBCDE-dA adducts was

[*]Corresponding Author at: Oregon State University Linus Pauling Institute, 473 LPSC, Corvallis, OR 97331, USA, david.williams@oregonstate.edu, phone:541-737-3277 fax:541-737-0497.

higher in skin than other target tissues such as spleen, lung and liver (oral dosing). These results document that Cyp 1b1 plays a significant role in bioactivation and carcinogenesis of DBC in a two-stage mouse skin tumor model and that loss of Cyp 1b1 has little impact on tumor response with BaP or CTE as initiators.

Graphical Abstract

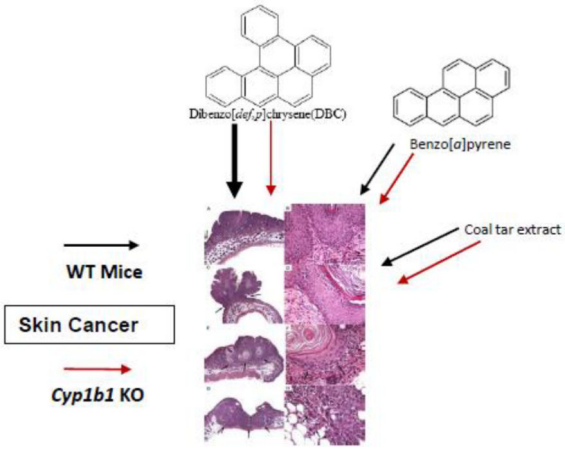

Keywords

PAHs; Cyp1b1; Relative Potency Factor; skin cancer; DNA adducts

1. Introduction

Polycyclic aromatic hydrocarbons (PAHs) are a class of organic chemicals containing two or more bonded aromatic rings. They can be petrogenic (petroleum sources) (Richter and Howard, 2000; Varnosfaderany et al., 2014) or pyrogenic (incomplete combustion of organic material) (Bostrom et al., 2002; Wang et al., 2014). Typical sources of PAHs are coal, crude and shale oil, tar, wood and tobacco smoke, smoked or charred foods, and fruits, vegetables, dairy products and grains through air or soil absorption (IPCS, 1998). Pyrogenic processes are by far the greatest contributor to environmental PAHs (Lima et al., 2005). The relative amounts of individual PAHs in a mixture vary depending on what type of combustion takes place (Poster et al., 2000). PAHs in the environment typically occur as mixtures of many types ranging in their number and structure of aromatic rings and subsequent degree of toxicity, from benign to extreme carcinogens (IARC 2010). As a result of the rapid increase in industrial development throughout the world, PAHs have been coined one of the re-emerging contaminants on a global scale. In light of this increased risk for potential human exposure, the Environmental Protection Agency (EPA) has been tasked with developing a strategy for estimating the risk of exposure to PAH mixtures (U.S. EPA, 2010). In order to do this it is imperative that researchers produce sound mechanistic data identifying the metabolic pathways for bioactivation of individual PAHs and mixtures to make accurate comparisons for potential risks to human health. Currently, EPA is evaluating a Relative Potency Factor (RPF) approach for estimating risk of exposure to PAH mixtures.

The RPF for risk assessment utilizes benzo[*a*]pyrene (BaP) as the reference (RPF=1), and estimates corresponding RPFs for each PAH which has sufficient published carcinogenicity data. BaP is one of the most studied PAHs found in the environment and is listed as a Group 1 or known human carcinogen by the International Agency for the Research on Cancer (IARC 2010). It is also listed in the top ten ATSDR list of priority pollutants (ATSDR, 2013). In addition to BaP our laboratory and others have studied the more potent animal carcinogenic PAH, dibenzo[*def,p*]chrysene (DBC), formerly labeled dibenzo[*a,l*]pyrene. Although DBC is currently classified as a 2A probable human carcinogen (IARC, 2010), this is mainly due to the lack of studies related to human exposures. When considering its potency in animal cancer models, EPA assigns DBC an RPF of 30.

BaP was first isolated from coal tar and long recognized as one of the drivers of mutagenesis and carcinogenesis in this PAH mixture (Cook et al., 1933; Phillips, 1983). The National Institute of Standards and Technology (NIST) standard reference material 1597a has a certified BaP mass fraction of 93.50 ± 1.40 mg/kg. DBC has been identified in coal tar (Mumford et al., 1987) and air particulates (DeRatt et al., 1987). It also is contained in 1597a with a certified mass fraction of 1.12 ± 0.17 mg/kg. The complete composition of PAHs (Magee and Sager, 2014) in 1597a coal tar, along with the recently revised individual RPFs and the resulting CTE estimate, is provided in Table 1. Using the new proposed values (Magee and Sager, 2014), the RPF for CTE is calculated as 400 mg/kg or 0.4 μg BaP_{eq} in the 1 mg CTE dose used in this study.

The chemical structure of parent PAHs makes them lipophilic. Therefore they are readily absorbed through biological membranes, and bioactivated through various metabolic pathways, converting the parent PAH to electrophilic metabolites, thus transforming inactive compounds into carcinogenic and mutagenic species (McClean et al., 2007; Fustinoni et al., 2010; Jacques et al., 2010; Crowell et al., 2011). Evidence of three separate pathways of PAH metabolism have been published in the scientific literature (reviewed in Wue and Warshawsky, 2005). The most thoroughly studied of these three entails a series of cytochrome P450 (CYP)-dependent oxygenations. CYP 1A1 and/or CYP 1B1 mediate the first epoxygenation. Hydrolysis by epoxide hydrolase produces two (±) BaP-7,8-dihydrodiols. A second CYP 1A1 or CYP 1B1 epoxygenation results in 4 enantiomers (±-*cis/trans*) of BaP 7,8-dihydrodiol-9,10-epoxide (BPDE) in the case of BaP or with DBC, the (±-*cis/trans*) of DBC-11,12-dihydrodiol-13,14-epoxide (DBCDE) (Shimada, 2006; Shou et al., 1996; Xue and Warshawsky, 2005). BaP and DBC contain “bay” and “fjord” regions, respectively, resulting in efficient covalent binding of the diol-epoxides to DNA or protein (Amin et al., 1995a; 1995b), assumed to be at least partially responsible for their potency as mutagens and carcinogens. Cavalieri and Rogan (1992; 1995) and Cavalieri et al. (2005), described a second mechanism involving formation of radical cations catalyzed by any number of peroxidases (including CYP) resulting in formation of a set of quinones (for BaP, predominantly at the 1,6-, 3,6- and 6,12- positions). Lastly, the *o*-quinone pathway is described in a recent review (Penning, 2014). Members of the aldo-keto reductase 1 (Akr 1) family mediate the formation of a catechol from the BaP- or DBC-dihydrodiol. Formation of the catechol sets up redox cycling through 1-electron reactions to an *o*-semi-quinone and *o*-quinone. This reversible cycle generates superoxide anion radical and, in the presence of

superoxide dismutase, hydrogen peroxide capable of causing oxidative DNA damage. All three of these mechanisms are capable of producing either stable or depurinating DNA adducts (Baird et al., 2005; Cavalieri et al, 2005; Zhang et al., 2014; Penning, 2014).

Our laboratory, along with Cavalieri et al., have demonstrated the marked potency of DBC, compared to that of BaP, in mouse models with lung and liver (Amin et al., 1995a), thymus and lung (Castro et al., 2009), breast and skin (Cavalieri et al., 1989; Gill et al., 1994; Higginbotham et al., 1993; Marston et al., 2001; Siddens et al., 2012) as target organs. BaP appears to be oxidized by both CYP 1A1 and CYP 1B1 whereas DBC is oxygenated by CYP 1B1 more so than by CYP1A1 (Shimada et al., 1999). Marston et al. (2001), showed that CTE, when co-administered with BaP or DBC, decreased the skin epidermal DNA binding and tumorigenicity compared to BaP or DBC alone. They postulated this could be due to competitive binding and inhibition of enzymes responsible for bioactivation of BaP and DBC by components in the complex mixture. Dermal application of DBC and DBC-11,12-dihydrodiol produced erythema in SENCAR mice suggesting induction of an immune hypersensitivity response that is not observed with other PAHs (Casale et al., 1997). This response could contribute to the increased carcinogenicity of DBC, relative to other PAHs, as well as relative slow repair of DBCDE-dA adducts (Kropachev et al., 2013; Spencer et al., 2009).

Transgenic and gene knockout animal models have become a useful tool for investigating the role of metabolizing enzymes and their effect on carcinogen bioactivation (Buters et al., 1999; Gonzalez, 2002). The critical role of CYP 1B1 in DBC bioactivation has been clearly defined using *in vitro* studies (Luch et al., 1998; Mahadevan et al., 2007) and *in vivo* animal models for lung, ovary, lymphoid tissue, skin, and endometria (Buters et al., 2002) as well as thymus, spleen, lung and liver through transplacental exposure (Castro et al., 2008).

Previous studies from our laboratory testing BaP, DBC and CTE in the FVB/N mouse two-stage skin tumor model, demonstrated that the previously utilized EPA RPFs underestimated the potency of DBC and CTE (Siddens et al., 2012). As the PAH mixture risk assessment (RPF) approach is driven by dermal exposures and there is some question from human xenograft studies on mice (human xenografts do not develop tumors following PAH exposure whereas surrounding mouse tissue is responsive), further mechanistic information was needed. In this study, we re-examine BaP, DBC and CTE as dermal carcinogens in the FVB/N mouse model employing animals wild-type for Cyp 1b1 (*Cyp1b1*$^{+/+}$), heterozygous mice (*Cyp 1b1*$^{+/-}$) and Cyp 1b1 null mice (*Cyp 1b1*$^{-/-}$).

2. Materials and methods

Caution: BaP and DBC are potent carcinogens and should be handled in accordance with National Cancer Institute (NCI) guidelines.

2.1. Chemicals

BaP (CAS no. 50-32-8) and DBC (CAS no.191-30-0) were purchased from Midwest Research Institute (Kansas City, MO). Coal tar extract (CTE, SRM 1597a) was purchased from the National Institute of Standards & Technology (Gaithersburg, MD). Trizol®, DNase

I, EDTA, Superscript™ III, RNase H, and Quant-iT ™ Picogreen® dsDNA assay kit were purchased from Life Technologies™ (Grand Island, NY). RNeasy and DNeasy kits and SYBR® Green Fluor Mastermix were from Qiagen (Alameda, CA) 12-*O*-tetradecanoylphorbol-13-acetate (TPA) was purchased from Sigma-Aldrich (St. Louis, MO). Acetone and toluene, HPLC grade was from Fisher Scientific (Pittsburgh, PA).

2.2. Skin tumor study

All procedures were conducted according to National Institutes of Health guidelines and were approved by the Oregon State University Institutional Animal Care and Use Committee. *Cyp 1b1*$^{-/-}$ (null) mice were back-crossed from a C57B6 strain (a generous gift from Frank Gonzalez at NCI) onto a FVB genetic background using wild type FVB/J from Jackson Laboratories (Bar Harbor, ME). The *Cyp 1b1* null animals used in this study were from offspring of the 7th backcross. *Cyp 1b1* genotype status was confirmed with PCR as described earlier (Castro et al., 2008). A combination of wild type litter mates from the same breeding and wild type FVB/J mice purchased from Jackson Lab were used in the *Cyp 1b1*$^{+/+}$ (wild type) groups. Six week old female mice were put on AIN93-G pelleted diet, Research Diets, Inc. (New Brunswick, NJ) until they were twelve weeks old. At this time they were switched to AIN93-M maintenance ration for the remainder of the experiment. Animals were housed in micro-ventilated racks, five animals per cage on a standard 12 h light/dark cycle, at 22°C and 40–60% humidity. At 7.5 weeks of age, mice were shaved on their dorsal surface and allowed to rest 48 h to confirm that animals were in the resting phase of the hair growth cycle. DBC and BaP were solubilized in toluene to make initiator dosing solutions. CTE (SRM 1597a) was received from NIST as an 8 mg/mL solution in toluene. The following initiation treatments were applied to mice, n = 18–25 (vehicle controls) and n = 30–35 (PAHs), by slowly pipetting solutions on the shaved area; toluene vehicle control (0.125 mL), BaP 400 nmol (100 μg), DBC 4 nmol (1.2 μg), or CTE (1 mg). Mice were initiated in two different cohorts randomly dispersed over all treatments. As PAHs (especially DBC) are light-sensitive, in order to prevent light-dependent breakdown of PAHs, we conducted the initiation in a darkened chemical hood. Immediately after dosing, the cages with dark tops were returned to a cage rack protected from light. Cages were not removed from those racks for the next 24 hours. Two weeks post-initiation, a 20-week promotion regimen was begun, treating animals twice weekly with TPA, 6.5 nmol (4 μg) in 0.10 mL acetone. Mice were observed and tumor incidence recorded weekly throughout the 20-week promotion interval. Following promotion, all animals were euthanized and necropsied. Skin tumors were trimmed, immediately fixed in buffered formalin, and embedded in paraffin. Haematoxylin and eosin-stained sections were analyzed by light-microscopy by a board-certified veterinary pathologist to confirm tumor incidence and degree of progression from papilloma to squamous cell carcinoma.

2.3. RNA extraction from DBC-initiated skin

Mice from each of the following genotypes, *Cyp 1b1*$^{+/+}$ (wt), *Cyp 1b1*$^{+/-}$ (het), and *Cyp 1b1*$^{-/-}$ (null), were given one initiation dose of either toluene vehicle control (0.125 mL) or DBC 4 nmol (1.2 μg) using the same technique as described in the tumor study. Epidermis/derm is was harvested from mice (n=4/treatment) at 2, 4, and 8 h post-initiation, placed in Trizol reagent, and snap-frozen in liquid N_2. Harvested frozen skin was placed in a 15-mL

sterile, disposable conical homogenizer, VWR Scientific Inc. (San Francisco, CA) and homogenized in 2 mL Trizol® reagent. RNA was extracted according to the manufacturer's instructions followed by a clean-up step using an RNeasy® mini kit. All samples were quantitated with a Nanodrop spectrophotometer, Thermo Scientific (Wilmington, DE). Acceptable A_{260}/A_{280} ratios were 2.0–2.1. Sample quality was confirmed by examining 18S and 28S peaks using an Agilent Technologies Bioanalyzer 2100 (Santa Clara, CA). RNA relative integrity numbers averaged 6.30 ± 0.44 or greater.

2.4. mRNA Expression Using Quantitative PCR

Expression of selected genes over a 2–8 h post-initiation time period was measured using quantitative PCR on cDNA template generated with Superscript™ III reverse transcriptase per manufacturer's instructions. Final reactions were diluted 1:10 with nuclease-free water. Published primer sequences (Table 2) were synthesized by Life Technologies Inc. (Grand Island, NY) and used at 600 nM in a 20 μL reaction. SYBR Green Mastermix was used on a BioRad iQ5 thermocycler, 1 cycle at 95°C for 5 min, 40 cycles at 95°C for 15 sec then annealed and extended 1 min, followed by a melt curve analysis to confirm a single product. Genes of interest were normalized to GAPDH and relative expression calculated by the $^{\Delta\Delta}$Ct method (Schmittgen and Livak, 2008).

2.5 DNA Extraction and Hydrolysis

Mouse epidermis/dermis (300 mg) from the same 8 h post-initiated animals as used in RNA extraction were homogenized in lysis buffer with a Brinkman Polytron (Kinematica AG Luzern, Switzerland) and DNA extracted with a Qiagen Genomic DNeasy Extraction kit. DNA was solubilized in nuclease-free water, quality confirmed by 260/280 ratios and quantity measured with a Nanodrop ND-1000 UV-Vis spectrophotometer (Nanodrop Technologies, Wilmington, DE). DNA was prepared for UHPLC-MS/MS as described in (Ruan et al., 2006) with some modification. Samples (100 μg in 0.45 mL water) were digested with 45 μL of 0.1 M $MgCl_2$ and 375 U (1.3 μL) DNase I for 1.5 h at 37°C followed immediately with 7.5 μL of 50 mM NaOAc, 5 mM $ZnCl_2$, pH 5.0, containing 7 U of nuclease P1 and incubated for 1.5 h at 37°C, and finally added 30 μL of 0.5 M Tris-HCl, 50 mM $MgCl_2$, pH 8.5, 30 U of alkaline phophatase (30 μL), and incubated for 1.5 h at 37°C. A 50 μL aliquot was reserved for base analysis and an internal standard (40 pg ^{15}N-labeled (±)-*anti*-*cis*-DBCDE-dA and (±)-*anti*-*trans*-DBCDE-dA) was added to the remaining portion. After addition of the internal standard absolute ethanol (600 μL) was added, samples were incubated at −20°C overnight and centrifuged at 14,000g for 10 min at 4°C. The supernatant was transferred to a new 1.7 mL microcentrifuge tube and evaporated to 50 μL under a nitrogen stream. Methanol (50 μL) was added to the samples to bring the volume to 100 μL (1 μg DNA/μL). Next the samples were filtered through a costar-X spin tube and transferred to an autosampler vial with 100 μL insert.

2.6 UHPLC-MS/MS Analysis

DBCDE-dA adducts were analyzed using a 4000 QTRAP hybrid triple quadrapole/linear ion trap LC-MS/MS system (AB Sciex, Redwood City, CA) with a Flexar UHPLC system (Perkin-Elmer, Waltham, MA) employing an Acuity UPLC BEH C_{18} 1.7 μm column

(Waters, Milford, MA). Solvent A (5 mM NH_4OAc + 0.1% formic acid in HPLC grade water) and solvent B (acetonitrile) were used in a gradient with a flow rate of 500 μL/min as follows: 1) 0.5 min 80% A and 20% B; 2) 6 min to 10% A and 90% B; 3) 0.1 min 10% A and 90% B; 4) 0.9 min wash out 10% A and 90% B. MS parameters were set as follows: electrospray ionization - positive mode; electrospray source temperature −600°C; declustering potential − 60 eV; collision energy − 30 eV; entrance potential − 10 eV; cell exit potential − 10 eV; collision activated dissociation gas - high; curtain gas −20 psi. Adducts were analyzed in multiple reaction monitoring (MRM) mode with the following transitions 604.2/335.0, 604.2/317.0, 604.2/289.1 (targeted adducts) and 609.2/335.0, 609.2/317.0, 609.2/289.1 (internal standards). Peak integration was performed using Analyst 1.5.2 Software (AB Sciex, Redwood City, CA).

2.7. UHPLC-MS/MS Calibration Curves

DNA from untreated tissue was prepared as described for experimental samples. One hundred μg of DNA was spiked with either unlabeled (±)-*anti*-*cis*-DBCDE-dA or (±)-*anti*-*trans*-DBCDE-dA adducts (0.1, 0.3, 3.0 pg/μL), and 0.4 pg/μL ^{15}N-labeled adducts.

2.8 HPLC Base Analysis

Digested DNA reserved for base analysis was analyzed using a Luna 3 μm C_{18} column (Phenomenex, Torrance, CA) with an Alliance 2695 HPLC (Waters, Milford, MA) and a 2996 photodiode array detector (PDA), Solvent A was 20 mM ammonium formate (pH 4.5), and solvent B was acetonitrile with a flow rate of 0.4 mL per min. The gradient used was 99% A and 1% B for 3 min, followed by a 12 minute ramp from 99% A to 60% A and 1% B to 40% B. A wavelength of 254 nm was chosen for sample detection. Deoxyguanosine (dG) and deoxyadenosine (dA) standards eluted at 9.3 and 10.2 min, respectively. A calibration curve for each standard was constructed and sample base levels were calculated by interpolation of the curve using Empower 2 software (Waters, Milford, MA).

2.9 Statistics

Time to first tumor was evaluated by cumulative tumor incidence function for each condition to account for any early non-cancer related mortalities in the study (Gooley et al., 1999). Cumulative incidence functions were calculated in R using the *cmprsk* package and estimating the probability of developing a tumor at time *t*, given that an animal has not yet developed a tumor, in the presence of competing risks (e.g. early mortality). Statistical significance among cumulative tumor incidence curves was determined by Gray's log rank test for equality (Gray, 1988). A proportional hazards model, which also accounts for competing risks, was utilized to calculate subdistribution hazards ratios (Fine and Gray 1999). Tumor multiplicity was evaluated for conditions with more than one tumor-bearing animal, thus the control group was not included. An exact Kruskal-Wallis test was conducted to evaluate possible cohort effects, which were potentially identified in two of three groups (p-values of 0.0514 and 0.02) and a possible cage effect for the CTE group (p-value of 0.029). Therefore, a generalized linear mixed model with Poisson conditional distribution and logit link function was fit to the data. The model's fixed effects included treatment and genotype (represented as 8 conditions) with cage and cohort included as

random effects. A mixed model assuming normality using the square root of tumor multiplicity as the response variable was also fit and produced similar results, so the Poisson model is presented for ease of interpretability. The *lme4* and *glht* packages in R were used to fit the model and conduct pairwise comparisons, respectively. A one-step adjusted p-value was calculated for the multiple pairwise tests (Hothorn et al., 2008). To determine if the number of tumors per animal, by tumor type, was different amongst the treatment groups, a generalized linear mixed model with a Poisson conditional distribution and logit link function was fit to data for each tumor type separately. The treatment and genotype combination group was included as a fixed effect and cage and cohort were included as random effects. qRTPCR data were compared for significance using Graphpad InStat ver. 3.05 software (San Diego, CA). Relative expression data were analyzed by comparing toluene treated with DBC treated per each genotype and time point using a Mann-Whitney two-tailed T test. Kruskal-Wallis with a Dunn post- test was used to separately compare variance across genotype and time. Statistical analysis for DBCDE-dA adduct formation was performed using One-way Analysis of Variance (ANOVA) with Tukey's multiple comparisons test (Prism 6.0, Graphpad, La Jolla, CA). A p-value of ≤ 0.05 was considered significant.

3. Results

3.1. Initiation and Progression of Tumors

Carcinogen initiation and progression were measured with several tumor end points; timing of first tumor (latency), number of tumors per tumor bearing animal (TBA), and tumor characterization by histopathology after 20 weeks of promotion. As previously documented (Siddens et al., 2012), DBC initiated tumors with greater efficacy and shorter latency (Figure 1), higher multiplicity (Figure 2). These tumors also exhibited a more aggressive phenotype (greater percentage of *in situ* carcinoma and squamous cell carcinoma) (Figure 3) than mice treated with BaP; even though the DBC dose was 100-fold lower based on molar equivalents or about 3-fold lower based on RPF. The percent tumor bearing animals for the BaP, DBC and CTE treatments (Figure 1) were found to be significantly different from genotype-matched controls ($p<5.048\times10^{-6}$) with little effect from early mortality on incidence (p=0.4145). When testing for differences in genotype for each treatment separately, only the DBC treatment group had significantly different cumulative tumor incidence functions between wt and null (p-value = 0.0074), while all other groups had p-values greater than 0.5 for this test (Table 3). Multiplicity in the wt mice treated with DBC was significantly increased compared to DBC-treated nulls (p=0.0289) with an estimated ratio of 1.950 (Table 3, Figure 2). Multiplicity in DBC-treated wt mice was also increased compared to all other treatments of wt mice (p<0.0062) (Figure 2). There was no effect of genotype on tumor multiplicity for BaP or CTE. There was also an effect of treatment on the distribution of tumor types observed in the study (Figure 3). DBC treatment of wt mice resulted in significantly more *in situ* carcinoma and squamous cell carcinoma compared to other wt treatment groups (p<0.004) and compared to nulls treated with DBC (p<0.001 and p=0.011, respectively, for each tumor type (Figure 4)). Interestingly, the relative yield of papillomas was lower in the present study with BaP and DBC compared to a previous study

in our laboratory (Siddens et al., 2012) whereas squamous cell carcinomas and carcinomas in situ were markedly higher.

Loss of Cyp 1b1 expression significantly reduced DBC dermal carcinogenicity when assessed by all four parameters. In contrast, loss of Cyp 1b1 expression slightly, although not significantly, enhanced the carcinogenicity of BaP in this model. The latency, incidence, multiplicity and phenotype of skin tumors induced by CTE was not impacted by loss of Cyp 1b1 and, as previously noted (Siddens et al., 2012), the carcinogenicity of CTE was much greater than would have been predicted from the RPF (0.4 μg BaP_{eq}, compared to 100 for BaP and 36 for DBC) (Table 1).

3.2. mRNA Response 2–8 Hour Post DBC Initiation in Cyp 1b1$^{+/+}$, Cyp 1b1$^{+/-}$ and Cyp 1b1$^{-/-}$ Mice

In order to assess the loss of *Cyp 1b1* expression on the mRNA levels of select genes coding for Phase I (Figures 5 and 7) and Phase II (Figure 6) enzymes involved in metabolism of PAHs, levels were quantified in *Cyp 1b1* wild-type mice and compared to their het and null siblings. qRTPCR (primer sequences in Table 2) was used to compare DBC-initiated skin to matched toluene-treated controls 2, 4 and 8 h after treatment. Similar to previous assays of mRNA levels 12 hours post-initiation, *Cyp 1a1* was not markedly induced at the earliest time point and declined over the next 6 h. The levels of *Cyp 1a1* mRNA were significantly ($p<0.05$) lower in the null mice at 4 and 8 h. In addition, all time points in the null groups had significantly lower expression compared to hets as did 2 h wt versus 2 h nulls ($p<0.05$), Figure 5, top panel). As previously observed (Siddens et al., 2012), DBC did not induce Cyp 1b1 in wt mouse skin (Figure 5, bottom panel). *Gst a1* mRNA levels, appeared to decline following DBC treatment (Figure 6). The loss of Cyp 1b1 had no significant effect on levels of *Gst a1* mRNA in skin, however hets had a significant increase in *Gsta1* at 8 h compared to 4 h ($p<0.05$, Figure 6, top panel). *Nqo1* was not significantly changed at any of these early time points with the one exception at 8 h in the null group, where it was down-regulated by DBC treatment ($p<0.05$, Figure 6, lower panel). Aldo-keto reductases of the 1c family were screened. Those showing measurable levels in a cDNA pool (Akr 1c12, Akr 1c13, Akr 1c14, Akr 1c18, Akr 1c19, Akr 1c20, and Akr 1c22) were further investigated. The pattern of *Akr 1c14* mRNA was similar to *Cyp 1a1*, declining over time following DBC treatment in wt and hets (Figure 7, top panel). Furthermore, loss of Cyp 1b1 expression in the null mice resulted in a significant ($p<0.05$) decrease of Akr 1c14 mRNA expression at all times measured (Figure 7, top panel). *Akr 1c19* levels were significantly higher in hets at 8 h compared to the 8 h nulls and conversely the 4 h hets were significantly ($p<0.05$) lower compared to 4 h nulls. However there were no differences when treated were compared to controls suggesting these genotype differences may not be treatment related (Figure 7, lower panel). Either no significant effects or too low of expression for reliable conclusions were observed for *Akr1c13, Akr1c18, Akr1c20, and Akr1c22* (data not shown.)

3.3. DNA Adducts 8 Hours Post DBC Initiation

Utilizing a highly sensitive stable-isotope dilution UHPLC-MS/MS assay (Harper et al., 2015, Figure 8) and ^{15}N-labeled (±)-*anti-cis*-DBCDE-dA and (±)-*anti-trans*-DBCDE-dA, standards kindly provided by Dr. Shantu Amin (Penn State University), we assayed at 8 h

DBC post-initiation levels of the two DNA adducts thought to be the most mutagenic and carcinogenic (Luch et al., 1999; Melendez-Colon et al., 1999). The levels of the (±)-*anti-cis*-DBCDE-dA adduct were significantly higher than (±)-*anti-trans*-DBCDE-dA (Figure 8, inset). Additionally, although not statistically significant, loss of Cyp 1b1 reduced the levels of both DBCDE-dA adducts in skin at 8 hours whereas there was no diminution in skin from the hets. These results are consistent with the reduced potency of DBC in *Cyp 1b1* null mice with respect to skin carcinogenesis.

4. Discussion

4.1. DBC and PAH Mixtures Exhibit Greater Carcinogenicity in Mouse Skin than Predicted by their RPFs: Role of Cyp 1b1

DBC in animal models is among the most potent carcinogenic PAHs (IARC, 2010). In a mouse transplacental model DBC administered to the dam (gestation day 17) at 15 mg/kg results in significant mortality from a very aggressive T-cell lymphoma (Yu et al., 2006). In the same model, BaP (50 mg/kg) and two different environmental PAH mixtures did not produce T-ALL in offspring. Enhanced lung tumors were observed at 10 months (Castro et al., 2008) though not to the degree produced by DBC. When the transplacental study was performed with crosses of *Cyp 1b1*$^{+/-}$ mice, no T-ALL was observed in the Cyp 1b1$^{-/-}$ offspring and the hets exhibited about 50% of the mortality of the Cyp 1b1$^{+/+}$ siblings (Castro et al., 2008). Thus, fetal expression of Cyp 1b1 was required for DBC-dependent transplacental mortality from T-ALL. Loss of Cyp 1b1 in the same study only slightly reduced DBC lung carcinogenicity.

In the mouse skin model (the most widely used for assessing PAH cancer risk), DBC and CTE exhibit much greater carcinogenicity, compared to BaP, than would be predicted based on the RPFs (Siddens et al., 2012 and current study). Loss of Cyp 1b1 increases the latency and reduces the incidence, multiplicity and aggressiveness of skin tumors initiated by DBC in the two-stage mouse model. In contrast, loss of Cyp 1b1 did not significantly impact the response with BaP or CTE (Figures 1–3). Based on the loss of both Cyp 1b1 and the marked reduction in skin Cyp 1a1 expression (Figure 5, top panel), the lack of decrease in BaP carcinogenesis in the Cyp 1b1$^{-/-}$ mice is somewhat surprising. With 7,12-dimethylbenz[a]anthracene as the initiator, Cyp 1b1 nulls exhibit reduced sensitivity to cancer at most targets, including skin (Buters et al., 1999). There was a complete elimination of skin hyperplasia in Cyp 1b1 null mice given DBC compared to wild type mice (Buters et al., 2002). Comparison to the present study is complicated by a different route of administration (oral) and different genetic background (C57Bl/6 and 129/Sv) in the previous studies.

4.2. Impact of Loss of Cyp 1b1 Expression on Levels of Select PAH Metabolizing Enzymes in Mouse Skin

The two major Cyps implicated in bioactivation of BaP and DBC in most mammalian tissues (Nesnow et al., 1998; Shimada, 2006; Shimada et al., 1999; Shou et al., 1996 including mouse skin (Kleiner et al., 2004) are Cyp 1a1 and Cyp 1b1. Cyp 1b1 is expressed in human skin (Svensson, 2009). Therefore it is not surprising that loss of global expression

of Cyp 1b1 resulted in reduced skin tumorigenesis especially given the concordant reduction in expression of Cyp 1a1 in skin (Figure 5, top panel). A previous study employing single, double and triple knockouts of the Cyp 1 family demonstrated that levels of Cyp 1a1 in other tissues were reduced in *Cyp 1b1* null mice through some unknown compensatory mechanism (Uno et al., 2006). In this same study, contrary to expectations, loss of Cyp 1a1 enhanced the toxicity of oral BaP apparently due to a reduced ability of these mice to eliminate BaP (steady state blood levels were 25-times higher in *Cyp 1a1*$^{-/-}$ mice compared to wt after 5 days of feeding BaP at 125 mg/kg). Previous studies by Dr. Baird's laboratory, utilizing microsomes from mouse epidermis (Courter et al., 2007; Marston et al., 2001) or human MCF-7 breast cancer cells Mahadevan et al., 2005a; 2005b), are consistent with the lack of induction of Cyp1a1 and Cyp1b1 by DBC; these studies were conducted 12–24 hours following DBC treatment.

Two key Phase II enzymes involved in detoxication of PAHs include Gst and Nqo 1, the former through conjugation of epoxides (Sundberg et al., 2002) and the latter by inhibition of redox cycling of catechols and quinones (Shen et al., 2010). There did not appear to be any compensatory regulation of expression of Gst a1 or Nqo 1 8 h post-initiation with DBC. Our recent studies comparing and contrasting BaP, DBC and CTE demonstrated that BaP and CTE in mouse skin impacted Ahr/Arnt, Nrf 2 and Sp 1 controlled signaling pathways (Tilton et al., 2015), whereas DBC did not. Dihydrodiols of PAHs (7,8-DHD for BaP and 11,12-DHD for DBC) can be converted to the corresponding catechols by AKR 1; the AKR 1C sub-family being important contributors (Quinn and Penning, 2008). Of the 7 mouse Akr1c members examined, loss of Cyp 1b1 only impacted Akr 1c14 mRNA expression 2–8 h after DBC treatment (Figure 7, top panel). The differences in *Akr 1c19* across time and genotype did not appear to be treatment related. Akr activity could be hypothesized to either enhance (Quinn and Penning, 2008) or repress PAH carcinogenicity. Conversion of the dihydrodiol reduces subsequent formation of the highly mutagenic and carcinogenic dihydrodiol-epoxide. Formation of the catechol, especially under conditions where Nqo levels are reduced, would enhance formation of reactive oxygen species (ROS) through 1 electron redox cycling with production of superoxide radical cation. Studies comparing the relative carcinogenicity of DBC-11,12-dihydrodiol-13,14-epoxide and DBC-11,12 dihydrodiol to DBC suggests that the parent compound could be as (Gill et al., 1994; Higginbotham et al., 1993) mutagenic/carcinogenic as these metabolites, again making conclusions about the relative mutagenicity of the two pathways uncertain. Unfortunately, in this study we did not assay ROS production nor assess any biomarkers of ROS cellular damage. Extrapolation of the importance of Akr 1c levels in mice to human risk is complicated by evidence suggesting that there is little homology between mouse and human members of the AKR 1c sub-family (Velica et al., 2009). It should be noted that the impact of loss of Cyp1b1 expression in mouse epidermis on expression of the various DBC-metabolizing enzymes examined in this study, while interesting, cannot be correlated to the final tumor response.

4.3. Levels of (±)-anti-DBCDE-dA Adducts 8 Hours Post-Initiation with DBC

Employing a highly sensitive stable-isotope dilution UHPLC-MS/MS assay (Harper et al., 2015, Figure 8) and ^{15}N-labeled standards, we have quantified the *cis* and *trans* isomers of

the (±)-*anti*-DBCDE-dA adduct, thought to be the major mutagenic and carcinogenic bioactivation products of DBC (Luch et al., 1999; Melendez-Colon et al., 1999). Unlike previous results from other DBC targets in the mouse (lung, liver, ovary) we found that the *cis* isomer predominated in skin from all three genotypes (*Cyp 1b1*$^{+/+}$, *Cyp 1b1*$^{+/-}$ and *Cyp 1b1*$^{-/-}$). The levels of adduction (15–20 (±)-*anti*-DBCDE-dAs/10^8 dA) are in the range seen in other studies (Harper et al., 2015). In the Cyp 1b1 nulls, the level of adduction was reduced by about 30% at the 8 h time point consistent with the reduced subsequent tumor yield in these mice. The caveat with these results is that only a single time point was examined; it may be that the *cis/trans* ratio would change over time if the DBC-dA stereoisomers had different rates of repair.

4.4. Conclusions

Consistent with previous results from our laboratory (Siddens et al., 2012) with the two-stage skin tumor model in the FVB/N mouse, DBC and CTE exhibit markedly greater carcinogenesis compared to BaP than would be predicted based on their calculated RPF values. To explore mechanistic explanations for this observation, we examined the impact of loss of Cyp 1b1, which our group and others have demonstrated is important in the carcinogenicity of a number of PAHs, including DBC. With DBC as the initiator, loss of Cyp 1b1 expression significantly enhanced the latency and reduced the incidence and multiplicity while shifting the tumor type to less aggressive phenotypes. As previously observed in another strain (Uno et al., 2006), there appears to be a compensatory mechanism such that Cyp 1a1 expression is reduced in the *Cyp 1b1* nulls, presumably reducing PAH bioactivation. We observed no consistent change in expression of genes which would contribute to detoxication of PAHs (e.g., *Gst a1* or *Nqo 1*). The reduction in *Akr 1c14* mRNA levels could reduce (±)-*anti*-DBCDE-dA formation but enhance ROS-dependent damage. The ratio of *cis/trans* isomers of (±)-*anti*-DBCDE-dA in skin was markedly higher than seen in other tissues. Additionally, both adducts were reduced in the *Cyp 1b1* null mice.

Limitations to this study include the fact that we only measured mRNA levels, rather than protein and utilized a limited time span. The use of other Cyp 1 knockouts, including the double and triple knockouts, may have shed more light on the relative contribution to skin carcinogenicity resulting from exposure to BaP, DBC or CTE. Conditional knockouts would have provided an additional advantage to the experimental design. Finally, the contribution of ROS in PAH-dependent skin cancer in this model was not assessed. What we can state with some certainty is that the RPF approach to risk assessment of PAH mixtures, and even single PAHs, is problematic. Cyp 1b1 contributes significantly to carcinogenesis in this model perhaps not only through loss of this bioactivation pathway but by additional alterations in expression of other PAH metabolizing enzymes through some, as yet, uncharacterized compensatory mechanism. Gene pathway analysis conducted by our laboratory strongly suggests that DBC alters a distinct set of signaling pathways compared to BaP and CTE which themselves share some commonalities but are also distinct. The carcinogenicity of DBC appears to be more related to its ability to alter p53 and Myc signaling compared to BaP and CTE which alter Ahr/Arnt, Nrf-2 and Sp1-controled gene expression (Tilton et al., 2015). Our studies reinforce previous observations that

environmental PAH mixtures have numerous mechanisms of action and risk assessment predictors need to take these into account.

Supplementary Material

Refer to Web version on PubMed Central for supplementary material.

Acknowledgments

The author would like to acknowledge the expert assistance of Jeff Morré in the Oregon State University Environmental Health Science Center Mass Spectrometry Core for his work with DNA adduct analysis, Ashley Kothen, Kristin Clausing, Jane Menino, and Sheila Cleveland for their care and handling of experimental animals. Cyp 1b1 knockout mice were a generous gift from Dr. Frank J. Gonzalez of the National Cancer Institute in Bethesda, MD. Dr. Arun Sharma and Dr. Shantu Amin at Penn State University, Hershey, PA provided standards for the UPLC/MS/MS analysis of DNA adducts. Pacific Northwest National Laboratory is a multi-program national laboratory operated by Battelle Memorial Institute for the DOE under contract number DE-AC05-76RLO1830.

Funding

This work was supported by the National Institute of Environmental Health Sciences through grants P42 ES016465, P30 ES000210 and T32 ES07060 and P01 CA90890 from the National Cancer Institute.

Abbreviations

Akr	aldo-keto reductase
ATSDR	Agency for Toxic Substances and Disease Registry
BaP	benzo[*a*]pyrene
CTE	coal tar extract
Cyp	Cytochrome P450
dA	deoxyadenosine
DBC	dibenzo[*def*,*p*]chrysene
DBCDE-A	dibenozo[*def*,*p*]chrysene-(±)-11,12-dihydrodiol-*cis* and *trans*-13,14-epoxide-deoxyadenosine
dG	deoxyguanosine
DOE	Department of Energy (USA)
EPA	Environmental Protection Agency (USA)
GST	glutathione-*S*-transferase
het(s)	heterozygous
IARC	International Agency for Research on Cancer
NIST	National Institute of Standards and Technology
NQO	NADPH quinone oxidoreductase
PAH	polycyclic aromatic hydrocarbon
ROS	reactive oxygen species

SRM	standard reference material
TPA	12-*O*-tetradecanoylphorbol-13-acetate
wt	wildtype

References

Amin S, Desai D, Dai W, Harvey RG, Hecht SS. Tumorigenicity in newborn mice of fjord region and other sterically hindered diol epoxides of benzo[g]chrysene, dibenzo[a,l]pyrene (dibenzo[*def*,*p*]chrysene), 4H–cyclopenta[def]chrysene and fluoranthene. Carcinogenesis. 1995a; 16:2813–2817. [PubMed: 7586203]

Amin S, Krzeminski J, Rivenson A, Kurtzke C, Hecht SS, el-Bayoumy K. Mammary carcinogenicity in female CD rats of fjord region diol epoxides of benzo[*c*]phenanthrene, benzo[g]chrysene and dibenzo[a,l]pyrene. Carcinogenesis. 1995b; 16:1971–1974. [PubMed: 7634428]

ATSDR. [accessed 12-31-2014] 2013. http://www.atsdr.cdc.gov/spl/resources/ATSDR_2013_SPL_Detailed_Data_Table.pdf.,

Baird WM, Hooven LA, Mahadevan B. Carcinogenic polycyclic aromatic hydrocarbon-DNA adducts and mechanism of action. Environm. Molec. Mutag. 2005; 45:106–114.

Bostrom CE, Gerde P, Hanberg A, Jernstrom B, Johansson C, Kyrklund T, Rannug A, Tornqvist M, Victorin K, Westerholm R. Cancer risk assessment, indicators, and guidelines for polycyclic aromatic hydrocarbons in the ambient air. Environm. Hlth. Persp. 2002; 110(Suppl 3):451–488.

Buters JT, Mahadevan B, Quintanilla-Martinez L, Gonzalez FJ, Greim H, Baird WM, Luch A. Cytochrome P450 1B1 determines susceptibility to dibenzo[a,l]pyrene-induced tumor formation. Chem. Res. Toxicol. 2002; 15:1127–1135. [PubMed: 12230405]

Buters JT, Sakai S, Richter T, Pineau T, Alexander DL, Savas U, Doehmer J, Ward JM, Jefcoate CR, Gonzalez FJ. Cytochrome P450 CYP1B1 determines susceptibility to 7, 12-dimethylbenz[*a*]anthracene-induced lymphomas. Proc. Natl. Acad. Sci. (USA). 1999; 96:1977–1982. [PubMed: 10051580]

Casale GP, Higginbotham S, Johansson SL, Rogan EG, Cavalieri EL. Inflammatory response of mouse skin exposed to the very potent carcinogen dibenzo[a,l]pyrene: a model for tumor promotion. Fund. Appl. Toxicol. 1997; 36:71–78.

Castro DJ, Baird WM, Pereira CB, Giovanini J, Löhr CV, Fischer KA, Yu Z, Gonzalez FJ, Krueger SK, Williams DE. Fetal mouse Cyp1b1 and transplacental carcinogenesis from maternal exposure to dibenzo(a,l)pyrene. Cancer Prev. Res. 2008; 1:128–134.

Castro DJ, Löhr CV, Fischer KA, Waters KM, Webb-Robertson BJ, Dashwood RH, Bailey GS, Williams DE. Identifying efficacious approaches to chemoprevention with chlorophyllin, purified chlorophylls and freeze-dried spinach in a mouse model of transplacental carcinogenesis. Carcinogenesis. 2009; 30:315–320. [PubMed: 19073876]

Cavalieri EL, Rogan EG. The approach to understanding aromatic hydrocarbon carcinogenesis. The central role of radical cations in metabolic activation. Pharmacol. Therapeut. 1992; 55:183–199.

Cavalieri EL, Rogan EG. Central role of radical cations in metabolic activation of polycyclic aromatic hydrocarbons. Xenobiotica. 1995; 25:677–688. [PubMed: 7483666]

Cavalieri EL, Rogan EG, Higginbotham S, Cremonesi P, Salmasi S. Tumor-initiating activity in mouse skin and carcinogenicity in rat mammary gland of dibenzo[*a*]pyrenes: the very potent environmental carcinogen dibenzo[a,l]pyrene. J. Cancer Res. Clin. Oncol. 1989; 115:67–72. [PubMed: 2921274]

Cavalieri EL, Rogan EG, Li KM, Todorovic R, Ariese F, Jankowiak R, Grubor N, Small GJ. Identification and quantification of the depurinating DNA adducts formed in mouse skin treated with dibenzo[a,l]pyrene (DB[a,l]P) or its metabolites and in rat mammary gland treated with DB[a,l]P. Chem. Res. Toxicol. 2005; 18:976–983. [PubMed: 15962932]

Cook JW, Hewett CL, Heiger I. The isolation of a cancer-producing hydrocarbon from coal tar. J. Chem. Soc. 1933:395–405.

Crowell SR, Amin SG, Anderson KA, Krishnegowda G, Sharma AK, Soelberg JJ, Williams DE, Corley RA. Preliminary physiologically based pharmacokinetic models for benzo[*a*]pyrene and dibenzo[*def*,*p*]chrysene in rodents. Toxicol. Appl. Pharmacol. 2011; 257:365–376. [PubMed: 22001385]

Courter LA, Musafia-Jeknic T, Fischer K, Bildfell R, Giovanini J, Pereira C, Baird WM. Urban dust particulate matter alters PAH-induced carcinogenesis by inhibition of CYP1A1 and CYP1B1. Toxicol. Sci. 2007; 95:63–73. [PubMed: 17060372]

DeRatt WK, Koojiman SALM, Gielsen JWJ. Concentrations of polycyclic hydrocarbons in airborne particles in the Netherlands and their correlation with mutagenicity. Sci. Total Environ. 1987; 66:95–114. [PubMed: 3317821]

Fine JP, Gray RJ. A proportional hazards model for the subdistribution of a competing risk. J. Amer. Stat Assoc. 1999; 94:496–509.

Fustinoni S, Campo L, Cirla PE, Martinotti I, Buratti M, Longhi O, Foa V, Bertazzi P. Dermal exposure to polycyclic aromatic hydrocarbons in asphalt workers. Occup. Environm. Med. 2010; 67:456–463.

Gill HS, Kole PL, Wiley JC, Li KM, Higginbotham S, Rogan EG, Cavalieri EL. Synthesis and tumor-initiating activity in mouse skin of dibenzo[a,l]pyrene syn- and anti-fjord-region diolepoxides. Carcinogenesis. 1994; 15:2455–2460. [PubMed: 7955091]

Gonzalez FJ. Transgenic models in xenobiotic metabolism and toxicology. Toxicol. 2002; 181–182:237–239.

Gooley TA, Leisenring W, Crowley J, Storer B. Estimation of failure probabilities in the presence of competing risks: new representations of old estimators. Stats. Med. 1999; 18:695–706.

Gray RJ. A class of K-sample tests for comparing the cumulative incidence of a competing risk. Annals Stats. 1988; 16:1141–1154.

Harper TA Jr, Morré JT, Lauer FT, McQuistan TJ, Hummel JM, Burchiel SW, Williams DE. Analysis of dibenzo[*def*,*p*]chrysene-deoxyadenosine adducts in wild-type and cytochrome P450 1b1 knockout mice using stable-isotope dilution UHPLC-MS/MS Mutat. Res. Gen. Toxicol. Environm. Mutag. 2015; 782:51–56.

Higginbotham S, RamaKrishna NV, Johansson SL, Rogan EG, Cavalieri EL. Tumor-initiating activity and carcinogenicity of dibenzo[a,l]pyrene versus 7,12-dimethylbenz[*a*]anthracene and benzo[*a*]pyrene at low doses in mouse skin. Carcinogenesis. 1993; 14:875–888. [PubMed: 8504480]

Hothorn T, Bretz F, Westfall P. Simultaneous inference in general parametric models. Biomet. J. 2008; 50:346–363.

IARC. Monographs on the evaluation of carcinogenic risks to humans. France: Lyon; 2010. Some non-heterocyclic polycyclic aromatic hydrocarbons and some related exposures.

IPCS. [Accessed January 27, 2015] 1998. http://www.inchem.org/documents/ehc/ehc/ehc202.htm.

Jacques C, Perdu E, Duplan H, Jamin EL, Canlet C, Debrauwer L, Cravedi JP, Mavon A, Zalko D. Disposition and biotransformation of ^{14}C-benzo(a)pyrene in a pig ear skin model: *ex vivo* and *in vitro* approaches. Toxicol. Lett. 2010; 199:22–33. [PubMed: 20696221]

Kleiner HE, Vulimiri SV, Hatten WB, Reed MJ, Nebert DW, Jefcoate CR, DiGiovanni J. Role of cytochrome P4501 family members in the metabolic activation of polycyclic aromatic hydrocarbons in mouse epidermis. Chem. Res. Toxicol. 2004; 17:1667–1674. [PubMed: 15606143]

Kropachev K, Kolbanovskiy M, Liu Z, Cai Y, Zhang L, Schwaid AG, Kolbanovskiy A, Ding S, Amin S, Broyde S, Geacintov NE. Adenine-DNA adducts derived from the highly tumorigenic dibenzo[*a*,*l*]pyrene are resistant to nucleotide excision repair while guanine adducts are not. Chem. Res. Toxicol. 2013; 26:783–793. [PubMed: 23570232]

Lima ALC, Farrington JW, Reddy CM. Combustion-derived polycyclic aromatic hydrocarbons in the environment—a review. Environm. Forens. 2005; 6:109–131.

Luch A, Coffing SL, Tang YM, Schneider A, Soballa V, Greim H, Jefcoate CR, Seidel A, Greenlee WF, Baird WM, Doehmer J. Stable expression of human cytochrome P450 1B1 in V79 Chinese hamster cells and metabolically catalyzed DNA adduct formation of dibenzo[a,l]pyrene. Chem. Res. Toxicol. 1998; 11:686–695. [PubMed: 9625737]

Luch A, Friesel H, Seidel A, Platt KL. Tumor-initiating activity of the (+)-(S,S)- and (-)-(R,R)-enantiomers of trans-11,12-dihydroxy-11,12-dihydrodibenzo[a,l]pyrene in mouse skin. Cancer Lett. 1999; 136:119–128. [PubMed: 10355740]

Magee, B.; Sager, S. [accessed 1/13/15] Proposed EPA changes in the toxicological assessment of benzo(a)pyrene and the potential impact on corrective actions at railroad sites. 2014. http://railtec.illinois.edu/RREC/presentations/A/02/11_Magee.pdf,

Mahadevan B, Keshava C, Musafia-Jeknic T, Pecaj A, Weston A, Baird WM. Altered gene expression patterns in MCF-7 cells induced by the urban dust particulate complex mixture standard reference material 1649a. Cancer Res. 2005b; 65:1251–1258. [PubMed: 15735009]

Mahadevan B, Luch A, Atkin J, Haynes M, Nguyen T, Baird WM. Inhibition of human cytochrome P450 1b1 further clarifies its role in the activation of dibenzo[a,l]pyrene in cells in culture. J. Biochem. Molec. Toxicol. 2007; 21:101–109. [PubMed: 17623886]

Mahadevan B, Marston CP, Dashwood W-M, Li Y, Pereira C, Baird WM. Effect of a standardized complex mixture derived from coal tar on the metabolic activation of carcinogenic polycyclic aromatic hydrocarbons in human cells in culture. Chem. Res. Toxicol. 2005a; 18:224–231. [PubMed: 15720126]

Marston CP, Pereira C, Ferguson J, Fischer K, Hedstrom O, Dashwood WM, Baird WM. Effect of a complex environmental mixture from coal tar containing polycyclic aromatic hydrocarbons (PAH) on the tumor initiation, PAH-DNA binding and metabolic activation of carcinogenic PAH in mouse epidermis. Carcinogenesis. 2001; 22:1077–1086. [PubMed: 11408352]

McClean MD, Rinehart RD, Sapkota A, Cavallari JM, Herrick RF. Dermal exposure and urinary 1-hydroxypyrene among asphalt roofing workers. J. Occup. Environm. Hyg. 2007; 4(Suppl 1):118–126.

Melendez-Colon VJ, Luch A, Seidel A, Baird WM. Cancer initiation by polycyclic aromatic hydrocarbons results from formation of stable DNA adducts rather than apurinic sites. Carcinogenesis. 1999; 20:1885–1891. [PubMed: 10506100]

Mumford JL, Harris DB, Williams K, Chuang JC, Cooke M. Indoor air sampling and mutagenicity studies of emissions from unvented coal combustion. Environm. Sci. Technol. 1987; 21:308–311.

Nesnow S, Davis C, Padgett W, George M, Lambert G, Meyers F, Allison J, Adams L, King LC. Metabolic activation of racemic and enantiomeric *trans*-8,9-dihydroxy-8,9-dihydrodibenzo[*a*,*l*]pyrene (dibenzo[*def*,*p*]chrysene) to dibenzo[*a*,*l*]pyrene-bis-dihydrodiols by induced rat liver microsomes and a recombinant human P450 1A1 system: the role of the K-region-derived metabolic intermediates in the formation of dibenzo[*a*,*l*]pyrene-DNA adducts. Chem. Res. Toxicol. 1998; 11:1596–1607. [PubMed: 9860506]

Penning TM. Human aldo-keto reductases and the metabolic activation of polycyclic aromatic hydrocarbons. Chem. Res. Toxicol. 2014; 27:1901–1917. [PubMed: 25279998]

Phillips DH. Fifty years of benzo(a)pyrene. Nature. 1983; 303:468–472. [PubMed: 6304528]

Poster DL, Alda MJLD, Wise SA, Chuang JC, Mumford JL. Determination of PAHs in combustion-related samples and in SRM 1597, complex mixture of PAHs from coal tar. Polycyc. Arom. Comp. 2000; 20:79–95.

Pratt-Hyatt M, Lickteig AJ, Klaassen CD. Tissue distribution, ontogeny, and chemical induction of aldo-keto reductases in mice. Drug Metabol. Disp. 2013; 41:1480–1487.

Quinn AM, Penning TM. Comparisons of (±)-benzo[*a*]pyrene-*trans*-7,8-dihydrodiol activation by human cytochrome P450 and aldo-keto reductase enzymes: effect of redox state and expression levels. Chem. Res. Toxicol. 2008; 21:1086–1094. [PubMed: 18402469]

Quinn AM, Harvey RG, Penning TM. Oxidation of PAH *trans*-dihydrodiols by human aldo-keto reductase AKR1B10. Chem. Res. Toxicol. 2008; 21:2207–2215. [PubMed: 18788756]

Richter H, Howard JB. Formation of polycyclic aromatic hydrocarbons and their growth to soot-a review of chemical reaction pathways. Prog. Energy Combust. Sci. 2000; 26:565–608.

Ruan Q, Kim HY, Jiang H, Penning TM, Harvey RG, Blair IA. Quantification of benzo[*a*]pyrene diol epoxide DNA-adducts by stable isotope dilution liquid chromatography/tandem mass spectrometry. Rapid Commun. Mass Spectrom. 2006; 20:1369–1380. [PubMed: 16557497]

Schmittgen TD, Livak KJ. Analyzing real-time PCR data by comparative C(T) method. Nature Protocols. 2008; 3:1101–1108. [PubMed: 18546601]

Shen J, Barrios RJ, Jaiswal AK. Inactivation of the quinone oxidoreductase NQO1 and NQO2 strongly elevates the incidence and multiplicity of chemically induced skin tumors. Cancer Res. 2010; 70:1006–1014. [PubMed: 20103645]

Shimada T. Xenobiotic-metabolizing enzymes involved in activation and detoxification of carcinogenic polycyclic aromatic hydrocarbons. Drug Metabol. Pharmacokin. 2006; 21:257–276.

Shimada T, Gillam EM, Oda Y, Tsumura F, Sutter TR, Guengerich FP, Inoue K. Metabolism of benzo[*a*]pyrene to trans-7,8-dihydroxy-7,8-dihydrobenzo[*a*]pyrene by recombinant human cytochrome P450 1B1 and purified liver epoxide hydrolase. Chem. Res. Toxicol. 1999; 12:623–629. [PubMed: 10409402]

Shou M, Krausz KW, Gonzalez FJ, Gelboin HV. Metabolic activation of the potent carcinogen dibenzo[a,l]pyrene by human recombinant cytochromes P450, lung and liver microsomes. Carcinogenesis. 1996; 17:2429–2433. [PubMed: 8968059]

Siddens LK, Larkin A, Krueger SK, Bradfield CA, Waters KM, Tilton SC, Pereira CB, Löhr CV, Arlt VM, Phillips DH, Williams DE, Baird WM. Polycyclic aromatic hydrocarbons as skin carcinogens: comparison of benzo[*a*]pyrene, dibenzo[*def*,*p*]chrysene and three environmental mixtures in the FVB/N mouse. Toxicol. Appl. Pharmacol. 2012; 264:377–386. [PubMed: 22935520]

Spencer WA, Singh J, Orren DK. Formation and differential repair of covalent DNA adducts generated by treatment of human cells with (±)-*anti*-dibenzo[*a*,*l*]pyrene-11,12-diol-13,14-epoxide. Chem. Res. Toxicol. 2009; 22:81–89. [PubMed: 19053321]

Sundberg K, Dreij K, Seidel A, Jernström B. Glutathione conjugation and DNA adduct formation of dibenzo[*a*,*l*]pyrene and benzo[*a*]pyrene diol epoxides in V79 cells stably expressing different human glutathione transferases. Chem. Res. Toxicol. 2002; 15:170–179. [PubMed: 11849043]

Svensson CK. Biotransformation of drugs in human skin. Drug Metabol. Dispos. 2009; 37:247–253.

Tilton SC, Siddens LK, Krueger SK, Larkin AJ, Löhr CV, Williams DE, Baird WM, Waters KM. Mechanism-based classification of PAH mixtures to predict carcinogenic potential. Toxicol Sci. 2015; 46(1):134–145.

Uno S, Dalton TP, Dragin N, Curran CP, Derkenne S, Miller ML, Shertzer HG, Gonzalez FJ, Nebert DW. Oral benzo[*a*]pyrene in *Cyp1* knockout mouse lines: CYP1A1 important in detoxication, CYP1B1 metabolism required for immune damage independent of total-body burden and clearance rate. Molec. Pharmacol. 2006; 69:1103–1114. [PubMed: 16377763]

Uno S, Dragin N, Miller ML, Dalton TP, Gonzalez FJ, Nebert DW. Basal and inducible CYP1 mRNA quantitation and protein localization throughout the mouse gastrointestinal tract. Free Radic. Biol. Med. 2008; 44:570–583. [PubMed: 17997381]

U.S. EPA. Development of a Relative Potency Factor (RPF) approach for polycyclic aromatic hydrocarbon (PAH) mixtures (External Review Draft). Washington, DC: U.S. Environmental Protection Agency; 2010. EPA/635/R-08/012A

Varnosfaderany MN, Bakhtiari AR, Gu Z, Chu G. Vertical distribution and source identification of polycyclic aromatic hydrocarbons (PAHs) in southwest of the Caspian Sea: most petrogenic events during the late Little Ice Age. Marine Pollut. Bull. 2014; 87:152–163.

Velica P, Davies NJ, Rocha PP, Schrewe H, Ride JP, Bunce CM. Lack of functional and expression homology between human and mouse aldo-keto reductase 1C enzymes: implications for modelling human cancers. Molec. Cancer. 2009; 8:121. [PubMed: 20003443]

Wang Z, Liu Z, Xu K, Mayer LM, Zhang Z, Kolker AS, Wu W. Concentrations and sources of polycyclic aromatic hydrocarbons in surface coastal sediments of the northern Gulf of Mexico. Geochem. Trans. 2014; 15:2. [PubMed: 24641695]

Xu M, Miller MS. Determination of murine fetal Cyp1a1 and 1b1 expression by real-time fluorescence reverse transcription-polymerase chain reaction. Toxicol. Appl. Pharmacol. 2004; 201:295–302. [PubMed: 15582647]

Xue W, Warshawsky D. Metabolic activation of polycyclic and heterocyclic aromatic hydrocarbons and DNA damage: a review. Toxicol. Appl. Pharmacol. 2005; 206:73–93. [PubMed: 15963346]

Yu Z, Loehr C, Fischer KA, Louderback M, Krueger SK, Dashwood RH, Kerkvliet NI, Pereira CB, Jennings-Gee J, Dance ST, Miller MS, Bailey GS, Williams DE. *In utero* exposure of mice to

dibenzo[*a*,*l*]pyrene produces lymphoma in the offspring: role of the aryl hydrocarbon receptor. Cancer Res. 2006; 66:755–762. [PubMed: 16424006]

Zhang SM, Chen KM, Sun YW, Aliaga C, Lin JM, Sharma AK, Amin S, El-Bayoumy K. Simultaneous detection of deoxyadenosine and deoxyguanosine adducts in the tongue and other oral tissues of mice treated with Dibenzo[a,l]pyrene. Chem. Res. Toxicol. 2014; 27:1199–1206. [PubMed: 24911113]

Highlights

- *Cyp1b1* null mice exhibit lower skin cancer sensitivity to DBC but not BaP or CTE
- Cyp1 b1 expression impacts expression of other PAH metabolizing enzymes
- *cis/trans*-DBCDE-dA ratio significantly higher in skin than spleen, lung or liver
- Potency of DBC and CTE in mouse skin is higher than predicted by RPFs

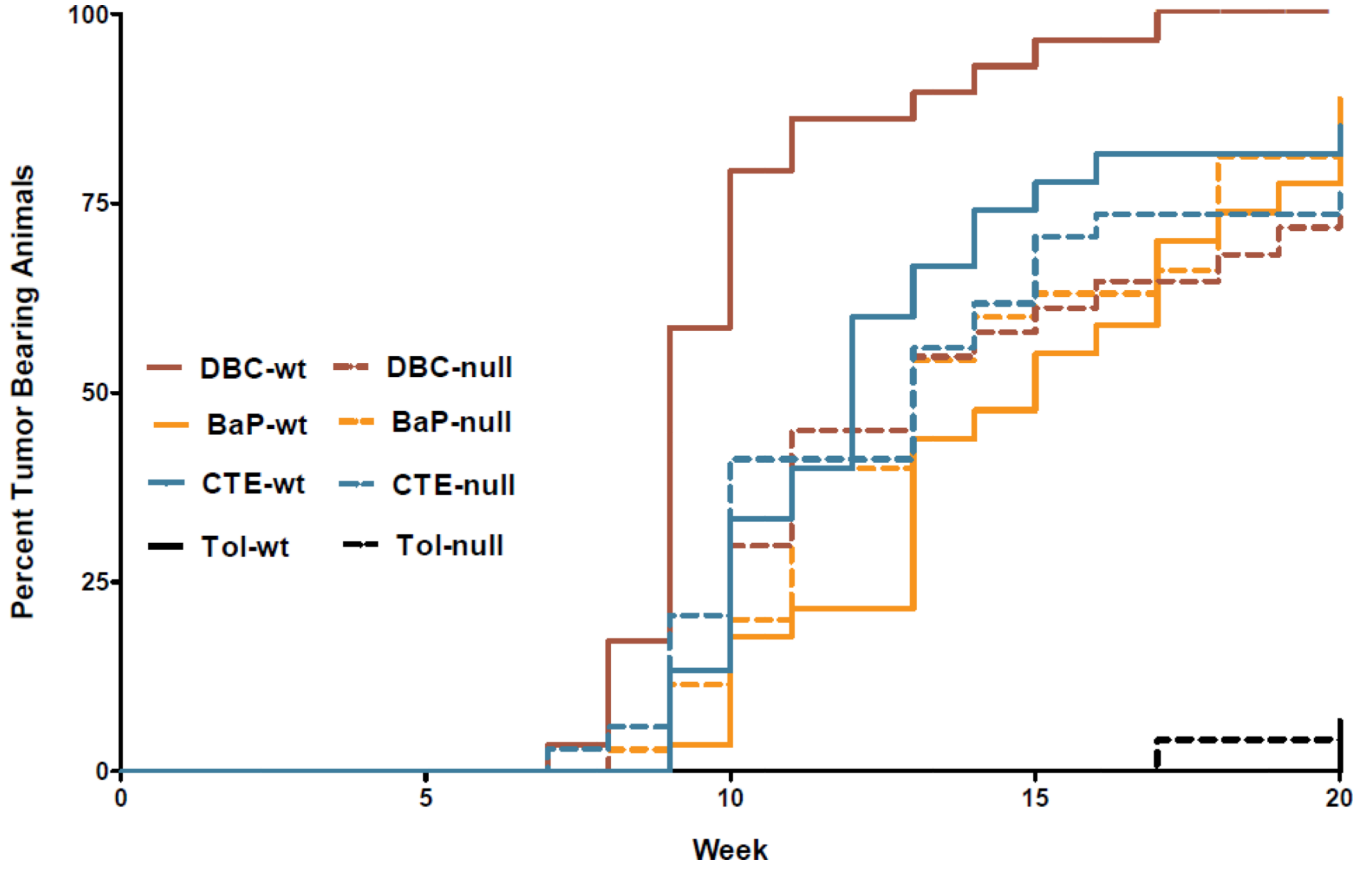

Figure 1.

Time to first tumor evaluated by cumulative tumor incidence function for each condition to account for any early non-cancer related mortalities in the study. The percent tumor bearing animals for all BaP, DBC and CTE treatments were significantly different from genotype-matched controls ($p<5.048\times10^{-6}$) as measured by Gray's log rank test for equality with little effect from early mortality on incidence ($p=0.4145$).

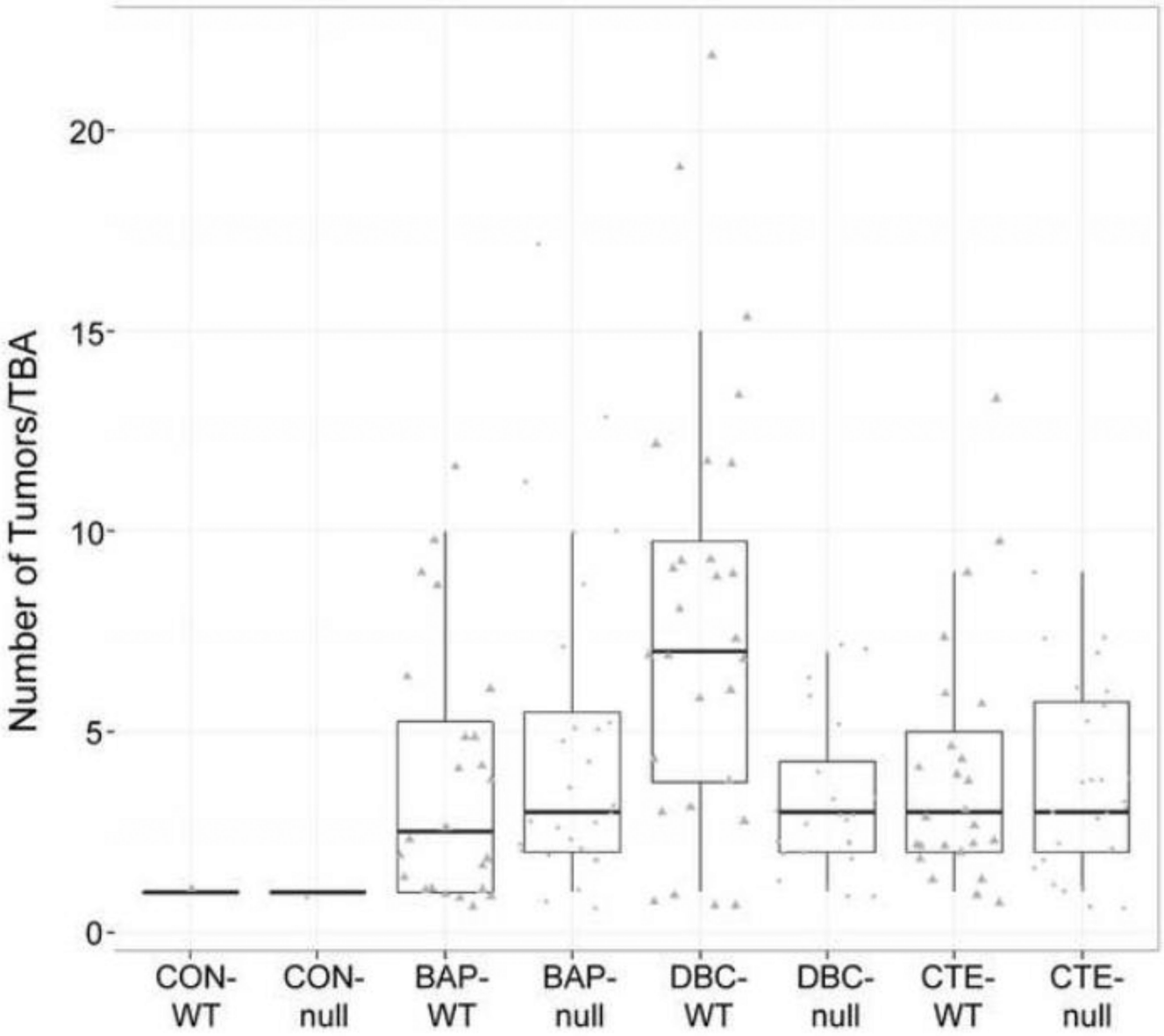

Figure 2.

Tumor multiplicity for tumor-bearing animals (TBA) by treatment and genotype. Points represent animals with at least one tumor at the end of the 20-week promotion period. *Cyp 1b1*$^{+/+}$ (wt) are triangles and *Cyp 1b1*$^{-/-}$ (null) are circles. Box plot shows median with the 25th and 75th percentiles and whiskers extending 1.5*interquartile range (75th-25th). Multiplicity in DBC-wt mice was significantly elevated compared to DBC-null mice (adjusted p=0.0289) or other wt treatment groups (adjusted p<0.0062) using a generalized linear mixed model with Poisson conditional distribution and logit link function.

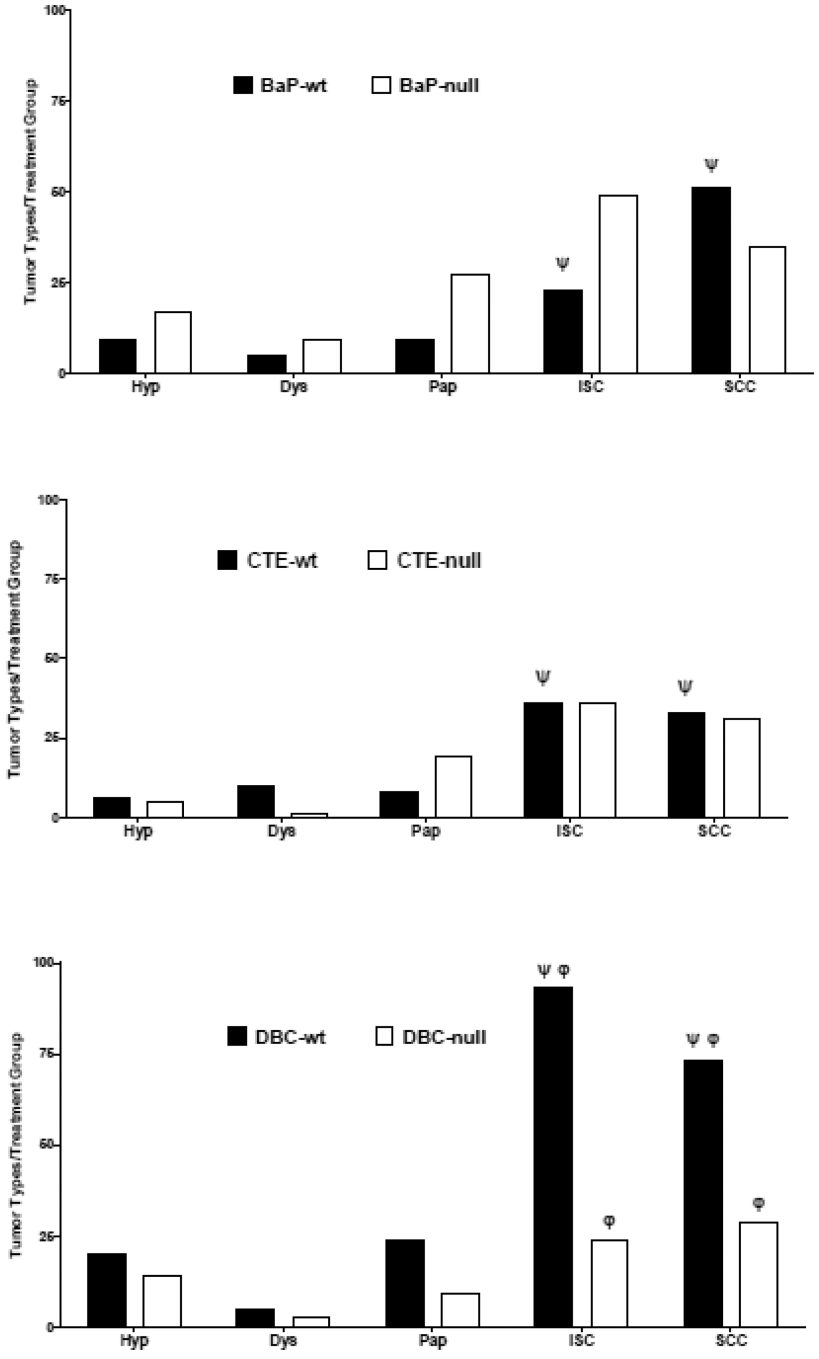

Figure 3.

Tumor progression as a distribution of types from hyperplasia (hyp)- dysplasia (dys)- papilloma (pap)- *in situ* carcinoma (ISC)- to squamous cell carcinoma (SCC) in each of the treatment groups. DBC treatment of wildtype mice resulted in significantly more *in situ* carcinoma and squamous cell carcinoma compared to other wildtype treatment groups ($p<0.004$) indicated by Ψ and compared to nulls treated with DBC ($p<0.001$ and $p=0.011$, respectively, for each tumor type ϕ).

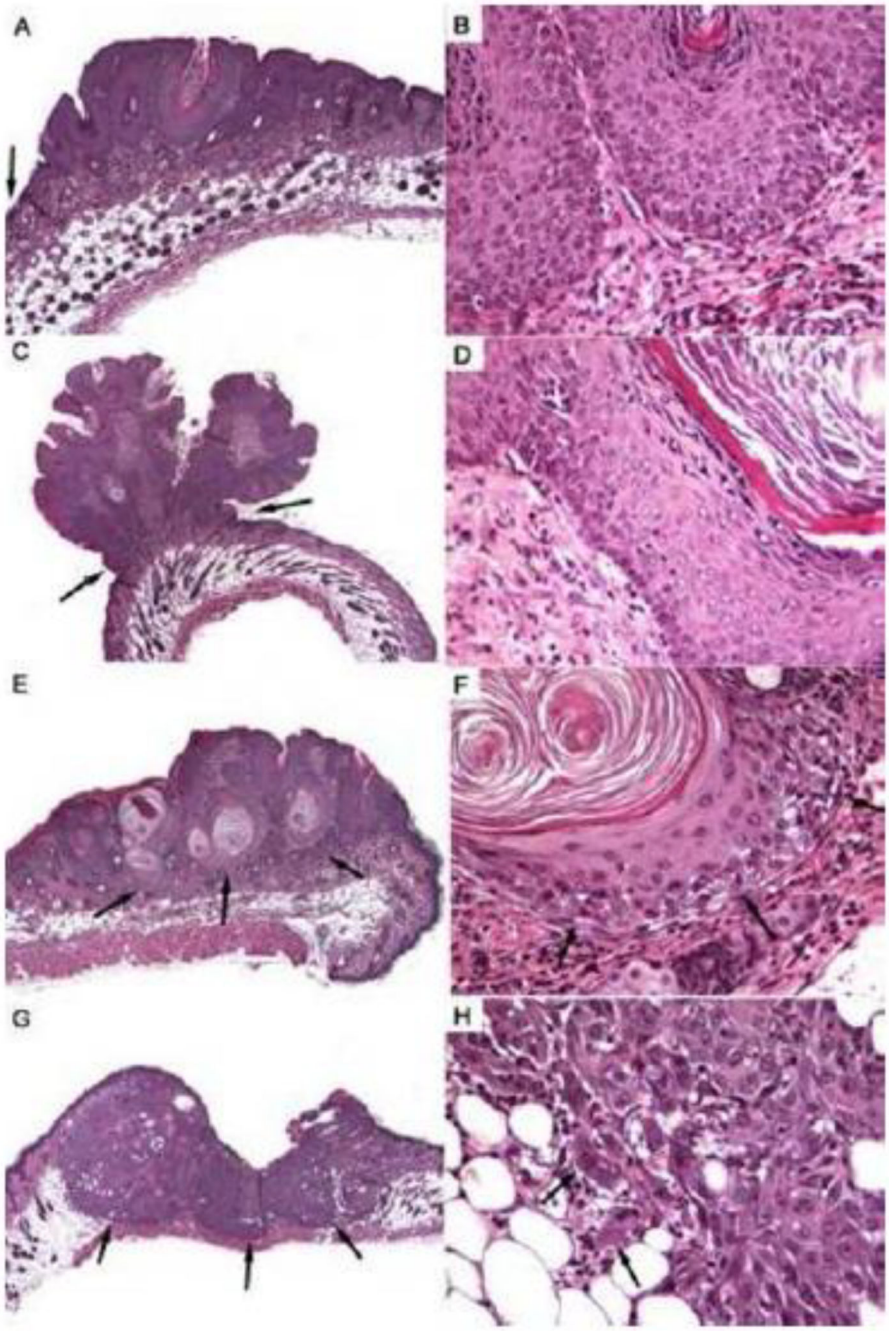

Figure 4.

Histological appearance of skin tumors showing the progression from hyperplasia (A,B), to papilloma (C,D), *in situ* carcinoma (E,F), and squamous cell carcinoma (G,H). Panels on the left provide a low-magnification view of the tumors (A,E,G at 100x; C at 40x). Note increased thickness of epidermis in hyperplasia in comparison to that in normal skin (A, arrow at the left margin) and the narrow base of the papilloma (C, arrows). In both hyperplasia (B) and papilloma (D), the physiological, gradual maturation of keratinocytes is maintained - from small basal cells in the lower half of panels B and D through the granular

cell layer to fully keratinized scales at the top (B) or right (D). Dermis in lower half is shown for orientation. While the in situ carcinoma is contained within the dermis (E, arrows) and has not breached the basement membrane zone (F, arrows) keratinocytes show some dysplasia and obvious dyskeratosis (F, note absence of granular cell layer and formation of keratin pearls). In contrast, the squamous cell carcinoma has deeply invaded the subcutis and is encroaching on the cutaneous muscle (G, arrows). Marked dysplasia can make it difficult to identify individual, invading neoplastic cells (H, arrows).

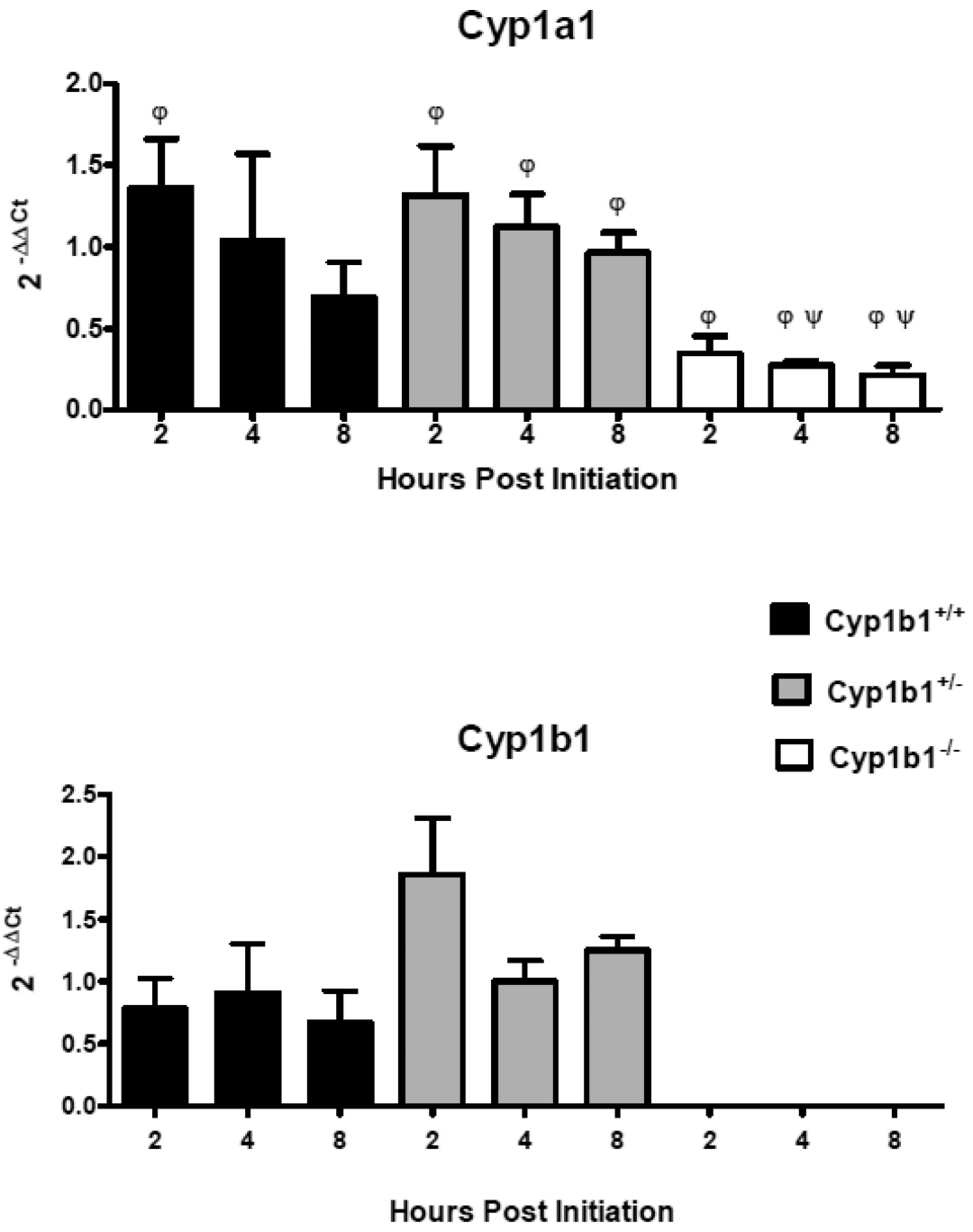

Figure 5.

Relative mRNA expression in selected P450 Cyp I metabolizing enzymes measured 2,4, and 8h post initiation with 0.125 mL toluene or 400 nmol DBC applied to the shaved dorsal surface of *Cyp 1b1*$^{+/+}$ (wt), *Cyp 1b1*$^{+/-}$ (het), and *Cyp 1b1*$^{-/-}$ (null) mice. qPCR using the $^{\Delta\Delta}$Ct method of expression in treated animals relative to toluene control are shown as mean ± SE of individual $2^{-(\Delta\Delta Ct)}$ values. ψ indicates significant difference between control and treated based on Mann Whitney two tailed test, φ indicates significant difference between genotypes using Kruskal-Wallis ANOVA with Dunn's post-test all p values <0.05.

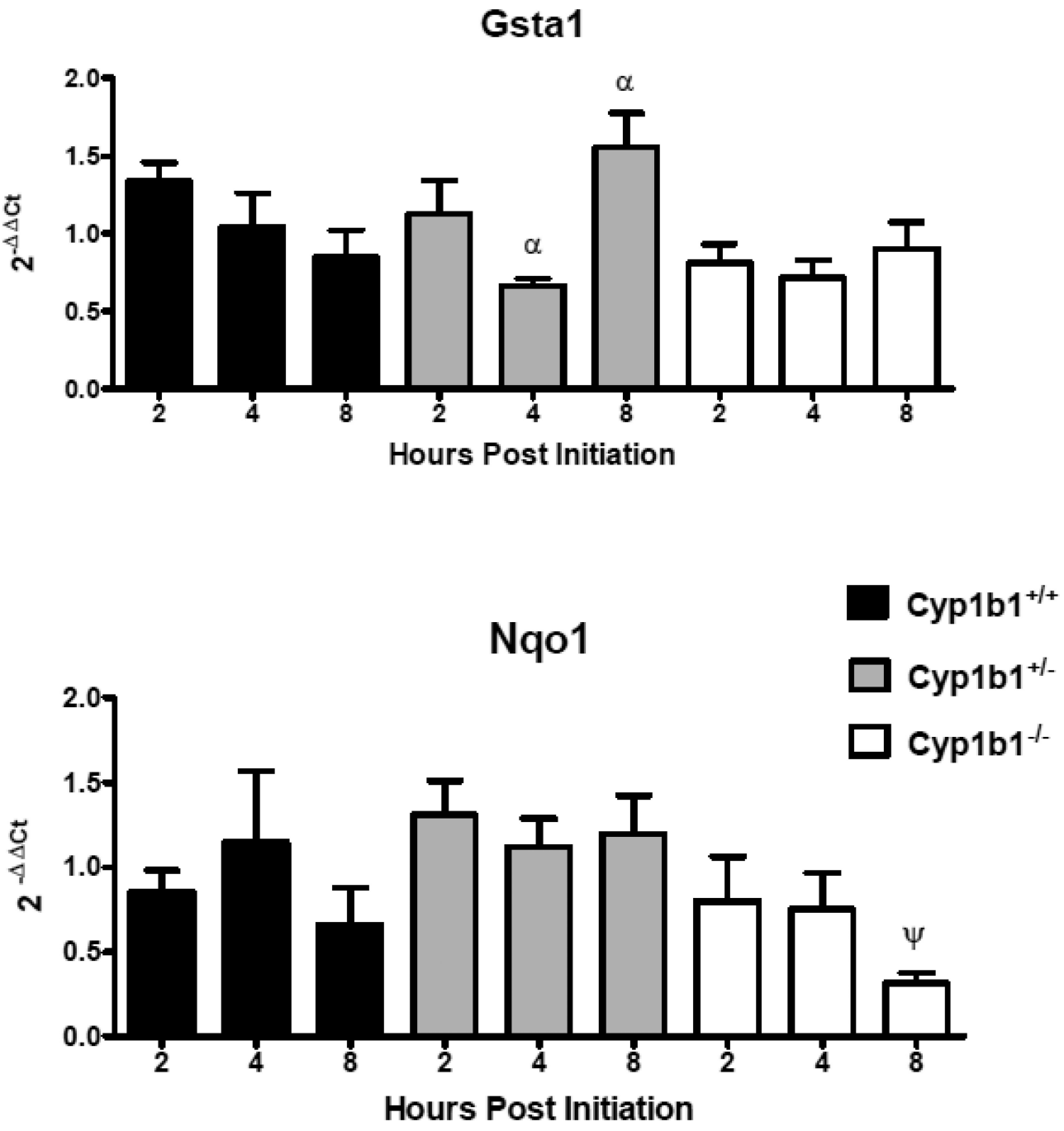

Figure 6.

Relative mRNA expression in selected Phase II metabolizing enzymes measured 2, 4,and 8 h post initiation with 0.125 mL toluene or 400 nmol DBC applied to the shaved dorsal surface of *Cyp 1b1*$^{+/+}$ (wt), *Cyp 1b1*$^{+/-}$ (het), and *Cyp 1b1*$^{-/-}$ (null) mice. qPCR using the $^{\Delta\Delta}$Ct method of expression in treated animals relative to toluene control are shown as mean ± SE of individual $2^{-(\Delta\Delta Ct)}$ values. ψ indicates significant difference between control and treated based on Mann Whitney two tailed test, α indicates significance between time points using Kruskal-Wallis ANOVA with Dunn's post-test all p values <0.05.

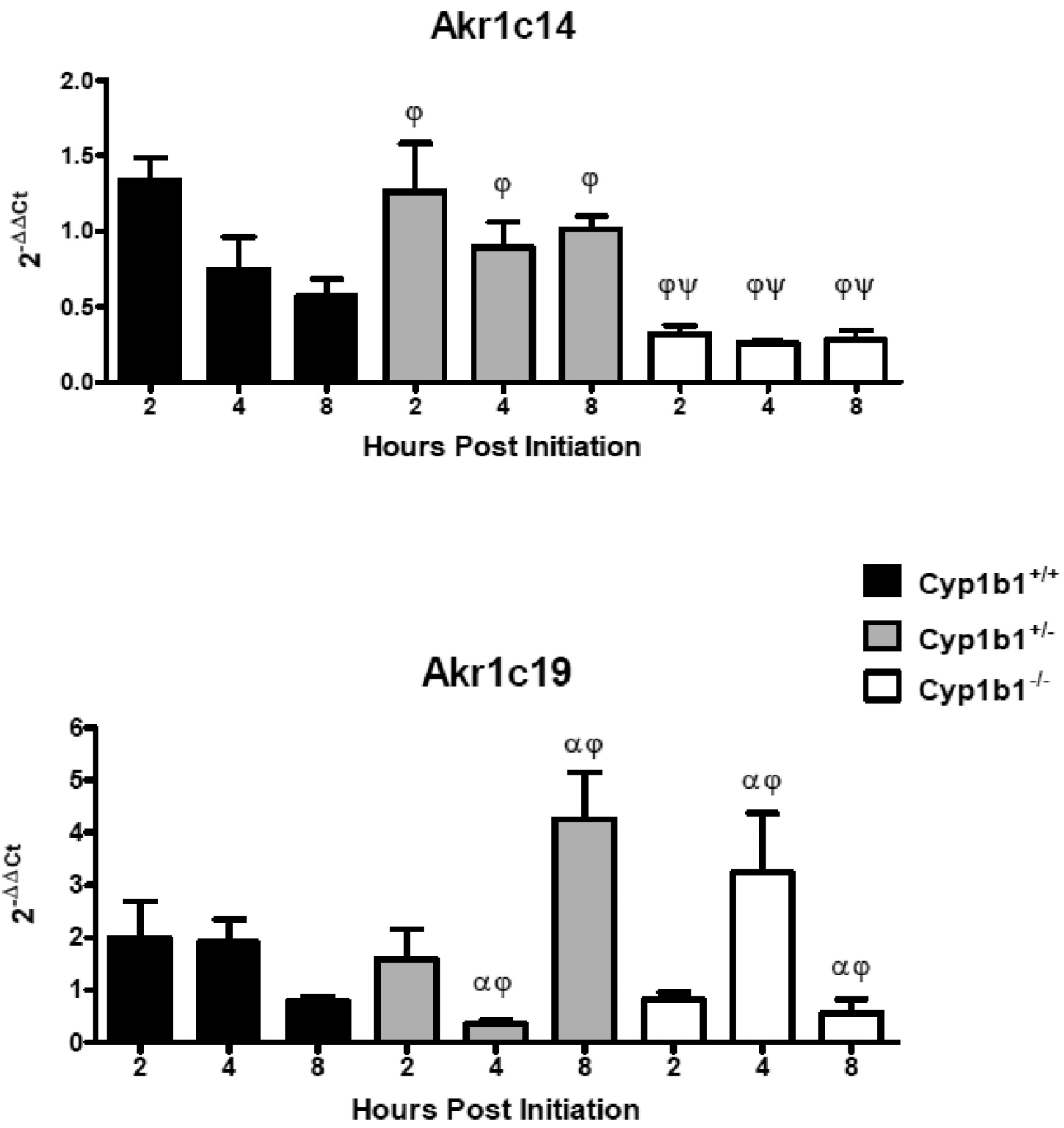

Figure 7.

Relative mRNA expression in selected *Akr 1c* metabolizing enzymes measured 2, 4, and 8 h post initiation with 0.125 mL toluene or 400 nmol DBC applied to the shaved dorsal surface of *Cyp 1b1*$^{+/+}$ (wt), *Cyp 1b1*$^{+/-}$ (het), and *Cyp 1b1*$^{-/-}$ *(null)* mice. qPCR using the $^{\Delta\Delta}$Ct method of expression in treated animals relative to toluene control are shown as mean ± SE of individual $2^{-(\Delta\Delta Ct)}$ values. ψ indicates significant difference between control and treated based on Mann Whitney two tailed test, φ indicates significant difference between

genotypes and α indicates significance between time points using Kruskal-Wallis ANOVA with Dunn's post-test; all p values <0.05 .

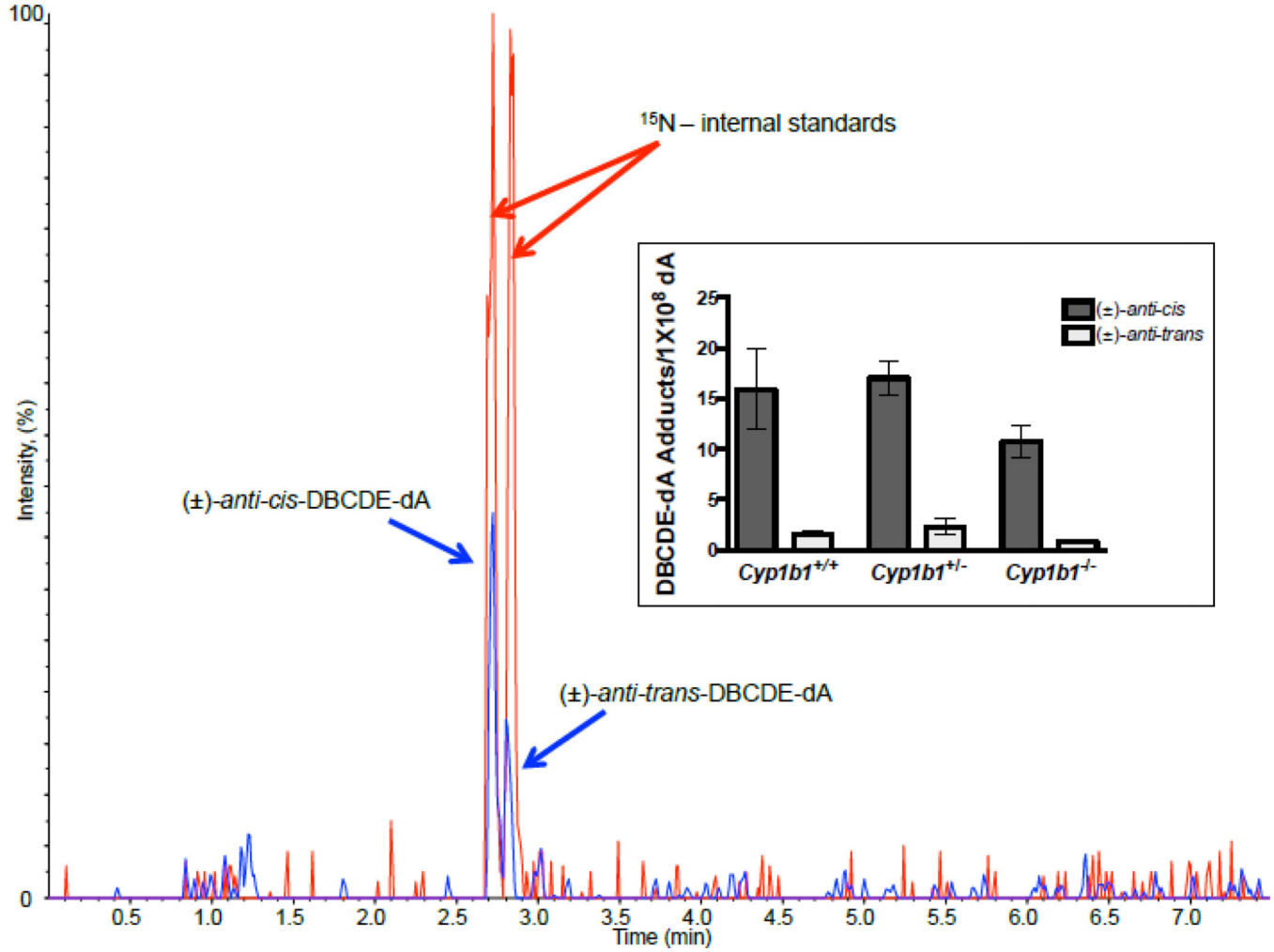

Figure 8.

Representative MRM chromatogram of DBCDE-dA adducts identified 8 hours post DBC initiation. The chromatogram indicates co-elution and detection of ^{15}N internal standards (red peaks (*m/z* 609.2 → *m/z* 335.0)) and target (±)-*anti-cis*- and (±)-*anti-trans*-DBCDE-dA adducts (blue peaks (*m/z* 604.2 → *m/z* 335.0)). Inset represents adduct quantitation for all 3 genotypes based on calibration curve and HPLC base analysis. One way ANOVA with Tukey's multiple comparison test indicate no significance difference in adduct formation between genotypes. However, the (±)-*anti-cis* isomer was formed at significantly greater levels than the (±)-*anti-trans* isomer in each group.

Table 1

Certified Mass Fractions for Selected PAHs in SRM 1597a*

Mass Fraction (mg/kg)[(a)]	
Acenaphthene 7.63±0.26	Indeno[1,2,3-*cd*]pyrene **(0.07)** 55.5 ±0.8
Acenaphthylene 263±7	2-Methylanthracene 10.4±0.2
	3-Methylchrysene 2.57±0.03
Anthracene 107±33	1-Methyldibenzothiophene 0.28±0.04
Benz[*a*]anthracene **(0.2)** 98.1 ±2.3	2-Methyldibenzothiophene 1.57±0.43
Benzo[*b*]chrysene 10.8±0.4	3-Methyldibenzothiophene 0.94±0.12
Benzo[a]fluoranthene 20.5±4.9	4-Methyldibenzothiophene 1.37±0.08
Benzo[*b*]fluoranthene **(0.8)** 66.1±4.4	8-Methyfluoranthene 6.33±0.78
Benzo[*ghi*]fluoranthene 13.5 ± 0.2	1-Methylnaphthalene 43.9±1.8
Benzo[*j*]fluoranthene **(0.3)** 36.5±2.4	2-Methylnaphthalene 95.0±2.9
Benzo[*k*]fluoranthene **(0.03)** 41.2±0.40	1-Methylphenanthrene 9.230.22
Benzo[*b*]nahtho[2,1-*d*]thiophene 2.41±0.21	2-Methylphenanthrene 19.1±1.1
Benzo[*b*]naphtho[2,1-*d*]thiophene 10.1±0.42	3-Methylphenanthrene 15.8±0.8
Benzo[*b*]naphtho[2,3-*d*]thiophene 3.68±0.59	4-Methylphenanthrene 1.04±0.13
Benzo[*b*]perylene 9.04±0.99	Naphthalene 1030±100
Benzo[*ghi*]perylene **(0.009)** 50.5±0.6	Naphtho[1,2-*b*]fluoranthene 8.6±2.0
Benzo[c]phenanthrene 11.0±0.5	Naphtho[1,2-*k*]fluoranthene 10.7±1.2
Benzo[*a*]pyrene **(1.0)** 93.5±1.4	Naphtho[2,3-*b*]fluoranthene 3.52±0.30
Benzo[*e*]pyrene 50.4±1.0	Naphtho[2,3-*k*]fluoranthene 2.07±0.06
Biphenyl 27.6±0.4	Naphtho[2,1-*a*]pyrene 10.2±0.9
Chrysene **(0.1)** 66.2±5.3	Naphtho[2,3-*a*]pyrene 4.29±0.89
Coronene 8.7±1.8	Naphtho[2,3-*e*]pyrene 4.31±0.44 **(0.3)**
4H-Cyclopenta[*def*]phenanthrene 52.4±4.5 **(0.3)**	Naphtho[1,2-*b*]thiophene 8.0±2.0
Cyclopenta[*c,d*]pyrene **(0.4)** 37.6±3.4	Naphtho[2,1-*b*]thiophene 6.05±0.21
Dibenz[*a,c*]anthracene **(4.0)** 4.35±0.21	Naphtho[2,3-*b*]thiophene 2.87±0.56
Dibenz[*a,h*]anthracene **(10.0)** 6.93±0.40	Pentaphene 4.6±1.5
Dibenz[*a, j*]anthracene 6.80±0.46	Perylene 24.6±0.9
Dibeno[*a,k*]fluoranthene 3.21±0.31	Phenanthrene 454±7
Dibenzo[*b,e*]fluoranthene 0.98±0.02	Picene 6.59±0.22
Dibenzo[*b,k*]fluoranthene 11.2±0.8	Pyrene 240±7
Dibenzo[*j,l*]fluoranthene 6.5±1.4	Triphenylene(g,h) 12.1±0.6
Dibenzo[*a,e*]pyrene **(0.4)** 9.08±0.39	
Dibenzo[*a,h*]pyrene **(0.9)** 2.57±0.30	
Dibenzo[*a,i*]pyrene 3.87±0.34 **(0.6)**	
Dibenzo[*a,l*]pyrene 1.12±0.17 **(30)**	
Dibenzo[*e,l*]pyrene 2.72±0.17	
Dibenzothiophene 17.7±0.4	
2,6-Dimethylnaphthalene 5.75±0.63	
1,7-Dimethylphenanthrene 1.43±0.10	

Mass Fraction (mg/kg)[(a)]
1,8-Dimethylphenanthrene 0.26±0.05
2,6-Dimethylphenanthrene 1.06±0.24
2,7-Dimethylphenanthrene 0.99±0.23
3,9-Dimethylphenanthrene 2.51±0.39
Fluorene 145±4
Fluoranthene **(0.08)** 327±7

* taken from https://www-s.nist.gov/srmors/certificates/1597A.pdf?CFID=5760584&CFTOKEN=1c554ace27253899-A2C20317-032C-6122-50A2525C1AA8AF67&jsessionid=f030f85734e4fd42e73015e41f5c6b543118

(a) Certified values are weighted means of the results from four to six analytical methods. The uncertainty listed with each value is an expanded uncertainty about the mean, with coverage factor 2 (approximately 95% confidence), except for benzo[*k*]fluoranthene for which a coverage factor of 8 was used, calculated by combining a between-method variance incorporating between-method bias with a pooled within-source variance following the ISO Guide.

EPAs Proposed Relative Potency Factors- taken from http://railtec.illinois.edu/RREC/presentations/A/02/11_Magee.pdf_Last accessed January 27, 2015

Total RPF= 400 mg/Kg

Table 2

Primers used in qPCR for selected PAH metabolizing enzymes.

Gene Name	Sequence	Source	Annealing Temp °C
Cyp1a1	(F) 5'-cctcatgtacctggtaacca-3' (R) 5'-aaggatgaatgccggaaggt-3'	1	60
Cyp1b1	(F) 5'-acatccccaagaatacggtc-3' (R) 5'-tagacagttcctcaccgatg-3'	1	60
Gsta1	(F) 5'-aagcccgtgcttcactacttc-3 ' (R) 5'-gggcacttggtcaaacatcaaa-3'	2	62
Nqo1	(F) 5'-aggatgggaggtactcgaatc-3' (R) 5'-aggcgtccttccttatatgcta-3'	2	62
Akr1c14	(F) 5'-tctcaagacctgcgtggttgca-3' (R) 5'-ggttccaaaccccagtgcaggg-3 '	3	60
Akr1c19	(F) 5'-atgcacctgctccatttggagag-3' (R) 5'-gctgtgcgtagaagtcatgacaca-3'	3	60
GAPDH	(F) 5'-tctccctcacaatttccatcccag-3' (R) 5'-gggtgcagcgaactttattgatgg-3'	4	59

[1] Uno et al., 2008

[2] www.pga.mgh.harvard.edu/primerbank/ Last accessed January 27, 2015

[3] Pratt-Hyatt et al., 2013

[4] Xu and Miller, 2004

Toxicol Appl Pharmacol. Author manuscript; available in PMC 2016 September 01.

Table 3

Influence of *Cyp1b1* genotype on tumor incidence and multiplicity.

Treatment	Genotype	Tumor Incidence[a]			Tumor Multiplicity		
		%[b]	p-value[c]	Ratio[d]	Mean±SE[e]	p-value[f]	Ratio[g]
BaP	*Cyp1b1*$^{+/+}$	88.89	1	1.172	3.88±0.67	0.495	0.682
	Cyp1b1$^{-/-}$	87.50			4.89±0.77		
CTE	*Cyp1b1*$^{+/+}$	86.21	1	1.017	3.96±0.62	0.983	0.837
	Cyp1b1$^{-/-}$	76.47			3.73±0.45		
DBC	*Cyp1b1*$^{+/+}$	100.00	7.409×10^{-3}	2.627	7.82±1.00	0.029	1.950
	Cyp1b1$^{-/-}$	72.73			3.29±0.41		

[a] Tumor incidence evaluated by cumulative tumor incidence function to account for early non-cancer related mortalities

[b] Percent tumor incidence at 20 weeks for each condition

[c] Statistical difference in tumor incidence between WT and null animals for each treatment group calculated by Gray's log rank test for equality adjusted for FDR (Gray 1988)

[d] Hazards ratio calculated for WT compared to null in each treatment group based on the proportional hazards model for the subdistribution of developing a tumor

[e] Tumor multiplicity calculated as the mean number of tumors per tumor-bearing animal (±SE)

[f] Statistical difference in tumor multiplicity between WT and null animals for each treatment group calculated using a generalized linear model to account for cage and cohort effects

[g] Estimated ratio of mean tumor multiplicity for WT compared to null